Multivalent patchy colloids for quantitative 3D self-assembly studies

Marlous Kamp,[*,†,‡] Bart de Nijs,[†,‡] Marjolein N. van der Linden,[†] Isja de Feijter,[¶] Merel J. Lefferts,[†] Antonio Aloi,[¶] Jack P. Griffiths,[‡] Jeremy J. Baumberg,[‡] Ilja K. Voets,[¶] and Alfons van Blaaderen[*,†]

†*Soft Condensed Matter, Debye Institute for Nanomaterials Science, Utrecht University, Princetonplein 1, 3584 CC Utrecht, The Netherlands.*

‡*NanoPhotonics Centre, Department of Physics, University of Cambridge, J J Thomson Avenue, Cambridge, CB3 0HE, United Kingdom.*

¶*Laboratory of Self-Organizing Soft Matter, Laboratory of Macromolecular and Organic Chemistry, Department of Chemical Engineering and Chemistry, Institute for Complex Molecular Systems, Eindhoven University of Technology, Post Office Box 513, 5600 MB Eindhoven, the Netherlands.*

E-mail: mkamp@cantab.net; A.vanBlaaderen@uu.nl

Abstract

We report methods to synthesize sub-micron and micron-sized patchy silica particles with fluorescently-labeled hemispherical titania protrusions, as well as routes to efficiently characterize these particles and self-assemble these particles into non-close-packed structures. The synthesis methods expand upon earlier work in literature, in which silica particles packed in a colloidal crystal were surface-patterned with a silane coupling agent. Here, hemispherical amorphous titania protrusions were successfully

labeled with fluorescent dyes, allowing for imaging by confocal microscopy and super-resolution techniques. Confocal microscopy was exploited to experimentally determine the numbers of protrusions per particle over large numbers of particles for good statistical significance, and these distributions were compared to simulations predicting the number of patches as a function of core particle polydispersity and maximum separation between the particle surfaces. We self-assembled these patchy particles into open percolating gel networks by exploiting solvophobic attractions between the protrusions.

INTRODUCTION

Patchy particles are colloidal particles with site-specific directional interactions[1–3] and, when subjected to Brownian motion, they are model particles analoguous to atoms with a valency[4] on a scale which is accessible to optical microscopy techniques. Patchy colloids have seen a steep rise in interest in the last decade[5–26] on account of their potential to form new types of bonds[4,27] and phases.[2,28–41] Until ∼5 years ago, experimental realization of patchy particles and in particular of their predicted phases lagged far behind theoretical descriptions, however recently experimental systems have started to catch up with theory and computer simulations. Firstly, the lag was due to the difficulty of synthesizing particles with multiple well-ordered patches (i.e. multivalent particles). Few synthetic methods allow to modify colloids site-specifically, especially in bulk. Most recent experimental systems presented are in fact still limited to Janus spheres, dumbbells and rods[27,42–45] and two-patch systems,[29] which can nevertheless result in very rich phase behaviour. A different strategy that can be used to create rich phase behaviour is mixing patchy and non-patchy particles or mixing various types of patchy particles.[16,46] A few beautiful systems with multiple patches have now been introduced.[47–53] Particle polydispersity, which is the variability in size and shape of particles and patches, also decreases the extent to which theory and experiments can be compared. Secondly, experiments lagged behind theory due to the difficulties in creating the required interaction strengths and depths to create the desired selectivity.[54] In the past five

years, however, patch-patch interactions have been created through mechanisms as diverse as DNA interactions,[14,18,49] supramolecular chemistry,[14,55,56] solvophobic interactions,[29,57] wetting-induced forces,[58] surface-liquid capillary bridging[59] and click reactions.[60] The studies referenced taken together demonstrate important progress in recent years in the synthesis of patchy particles and the inter-particle interactions required to create new phases.

A practical difficulty in studying multivalent patchy particles is that, to accurately study such systems by imaging techniques in real time, in 3D and *in situ*, it is essential to be able to distinguish the core and the patches in the imaging technique used. Many details that would be available from a quantitative real space analysis and would allow direct comparison with theory and simulations would not be available through the use of scattering techniques. This point is rather underexposed in the struggle to synthesize monodisperse systems with the desired interaction strengths, and will be addressed in the current work.

Even with the progress in experimental realization of patchy particles, there are still unexplored or underexplored predictions and aspects first introduced by theoretical calculations and simulations studies, such as the behaviour of patchy particles at low volume fractions,[28,61] out-of-equilibrium,[62,63] and on substrates[64–67]. In this work we focus on particles with high co-ordination numbers of up to twelve patches, which are also regularly placed, reflecting neighboring particles inside a colloidal crystal. Several recent theoretical studies have addressed self-assembly of patchy particles with high coordination numbers. For example, Reinhardt *et al.* found that these can form regular/crystalline structures through patch-patch interactions, however the free-energy barrier to nucleation is considerably higher than for e.g. tetrahedral particles, requiring higher supersaturation.[68] Newton *et al.* demonstrated that patchy particles with a higher valency but weaker interactions form structures with fewer defects than particles with a lower valency and stronger interactions.[69] Moreover, a number of theoretical studies have shown that patchy particles of intermediate and high valency can form low-density gel networks.[25,28,70–73] Such systems were observed experimentally in clay particle dispersions,[74] and we will touch upon the creation of such systems

in this work as well. Another concept that was initially introduced in a theoretical paper is that of inverse patchy particles (IPCs),[15,75–77] where patches adhere to the anti-patch of other patchy particles. Experimental examples of IPCs have recently been presented by van Oostrum *et al.*[78] and Sabapathy *et al.*[79]

In this paper, we describe the development of a system of multivalent patchy particles with distinguishable fluorescently-labeled cores and protrusions, the large-scale quantitative characterization and analysis of these systems using confocal microscopy, as well as the self-assembly of these patchy particles into gel structures. Our synthesis methods extend upon earlier work by Wang *et al.*[47] and by Bae *et al*,[48] who grew, respectively, (non-labeled) silica and titania protrusions onto silica colloids. In the methodologies developed by these groups, use was made of the fact that for touching particles in e.g. a packing of ball bearings the coordination numbers and local symmetries can be determined by poring a paint in and letting this dry, a method followed by Bernal and others many decades ago.[80] The reason being that the dried paint could not reach into the regions where particles touched or were very close to touching (the diameter of the rings formed were even a measure of how close the particles were). In the procedure we used, the paint is replaced by a silane coupling agent that can coat the silica surface exposed, but not where particles are touching each other. We used crystalline packings of the silica colloids, however, clearly the method can immediately be applied to create less regular patch distributions if we instead had used glasses, where the number of neighbors is almost the same as that in close-packed crystals.[81] After the coating reaction, the silica particles in the close-packed colloidal crystals can still be redispersed as single particles if enough energy is used, for instance by sonication and if the size is larger than several hundred nm such that shear can create strong enough forces. Already the redispersed system is composed of patchy colloids as the bare and silane coupling agent covered surfaces have different properties, like surface tension and charge density. It has been shown that by the right choice of silane coupling agent, both extra silica and/or titania can be deposited specifically onto the bare silica patches forming patches with also a geometric component

4

to the patchiness. We demonstrate how confocal microscopy, using the fluorescent labeling of cores and patches, can be harnessed to quantitatively analyze the numbers of patches per particle for large numbers of patchy partices. As we expected the number of patches to be strongly affected by polydispersity, we compared our experimental results and analysis to numerical simulations; we find good agreement. Finally, with the silane modified silica core and pristine titania patches, we explored attractions caused by both van der Waals forces and opposite surface charges, in the presence of generally low ionic strengths, enabling charge repulsions to also play a role. We study the self-assembly of these patchy particles in low-polar solvents, and find that the colloids form open, percolating structures, where the dispersion medium determines the nature of the patch-patch interactions.

RESULTS & DISCUSSION

Silica protrusions on sub-micron and micron-sized partices

Following Wang and coworkers,[47] silica particles were chemically patterned by immersing a
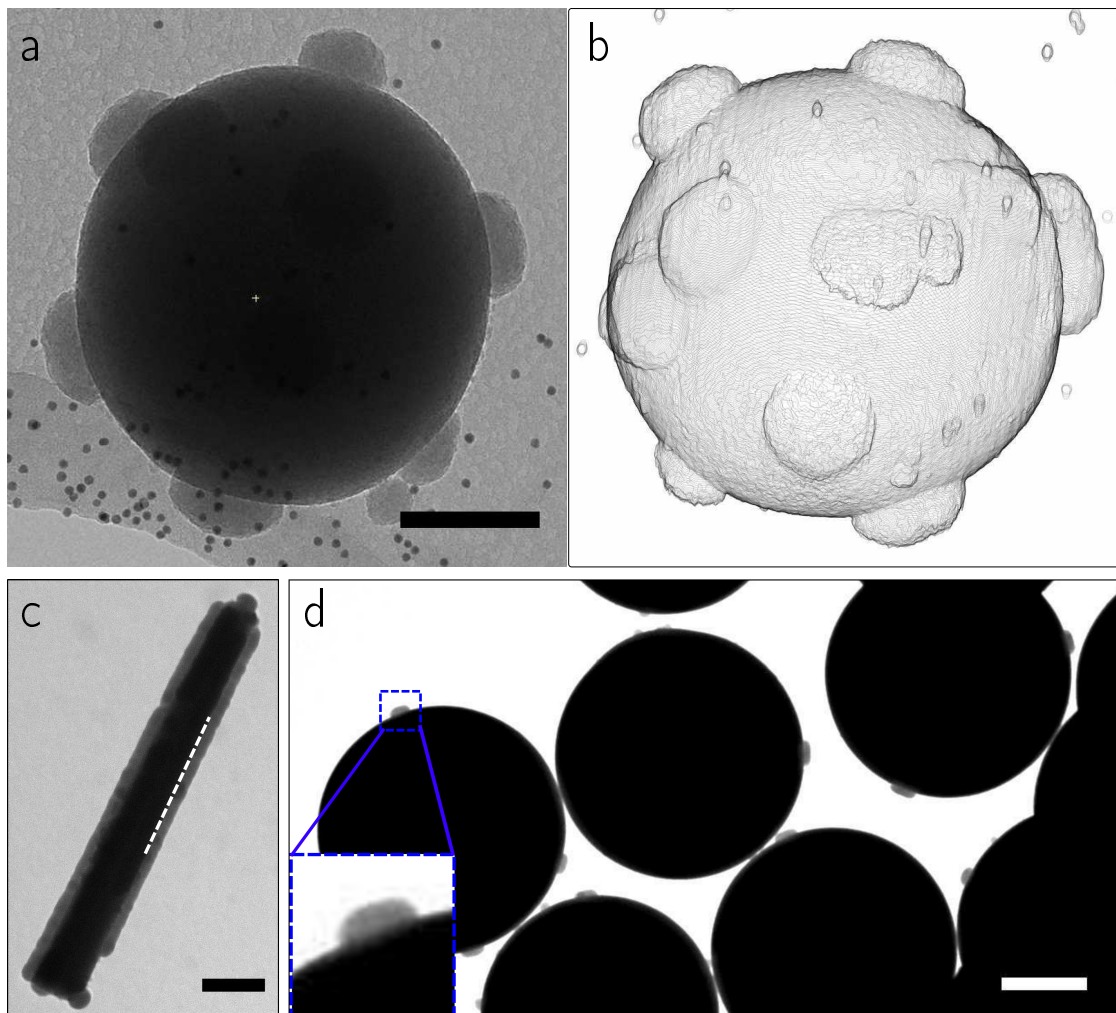

Figure 1: **Typical transmission electron microscopy (TEM) micrographs of silica particles with silica protrusions** fabricated by the annealing method with a silane coupling agent [3-methacryloxypropyltrimethoxysilane (MPTMS)] patterning[47] for sub-micron-sized and micron-sized core particle sizes. (a) Silica protrusions on a sub-micron silica particle (average particle size 411 ± 4 nm, polydispersity 4%). The black dots are gold markers for the tomographic reconstruction. (b) Surface rendering of a tomographic reconstruction of the particle in a obtained via electron tomography. (c) TEM micrograph of a fluted rod with 6 protrusions. The dotted line serves as a guide to the eye for the edge of one of the protrusions. (d) Silica protrusions on micron size silica particles ($1.43 \pm 0.02\,\mu$m, polydispersity 2%). The annealing temperature during synthesis was $500\,°$C (10h) for this sample. Scale bars denote (a) 100 nm, (c) 300 nm and (d) 500 nm.

dried (and thus close-packed) and annealed colloidal crystal of sub-micron size particles in an ethanolic reaction medium containing the silane coupling agent 3-methacryloxypropyltrimethoxysilane (MPTMS). After the colloidal crystal was redispersed as single particles by sonication, well-defined silica protrusions were grown onto these patterned colloids, with little to no silica deposition elsewhere on the colloid's surface (the 'antipatch'). Typical images of the product particles are shown in Figs. 1a,b. For several particles, all protrusions were visualized by means of Electron Tomography (ET),[82] see Fig. 1b and Supplementary Videos SV1-3. This technique circumvents the occlusion of the bottom of the particle that occurs in Scanning Electron Microscopy (SEM),[48] and to our knowledge ET is used here for the first time on such patchy particles. In agreement with ref. 48, the number of protrusions on each particle was in general below twelve (Figures S1,S2), the coordination number in a close-packed colloidal crystal of purely monodisperse spheres. Possible causes for this discrepancy between the maximum and the observed number of protrusions per particle are crystal defects in the colloidal crystal used for synthesis,[83] and more importantly the fact that the colloids from which these patchy particles were synthesized were not perfectly monodisperse,[48] a point which we will discuss in more detail later.

To demonstrate the versatility of the approach, we also prepared patchy rod-like silica particles in this manner. In short, rod-like particles developed in our group[84,85] were allowed to sediment and form a smectic phase, and the colloidal crystal of rods was dried, annealed, and treated with MPTMS. After redispersion of the particles, silica was grown onto the non-modified patches, resulting in fluted rod-like particles with silica wings (Fig. 1c and SI§2/Fig. S3).

The synthesis procedure was also extended to silica core particles larger than a micron (Fig. 1d and SV2), because larger colloids and larger patches are more suitable for quantitative 3D fluorescence microscopy studies.[81] In micron-sized particles, we observed comparatively more protrusions when the colloidal crystal was annealed at a lower annealing temperature (600 °C instead of 750 °C) (Fig. S4), most likely because there is less shrinkage

of the particles at these reduced temperatures.[86–88] In further experiments we used an 'anhydrous' synthesis route (see *Methods*) that avoids annealing by using an apolar solvent as reaction medium for surface functionalization of the colloidal crystal (since colloidal silica crystals were found to redisperse too easily upon immersion in more polar solvents). This anhydrous synthesis route avoided particle shrinkage and this observed variability, while in addition enabled fluorescently labeled silica particles to remain fluorescent.
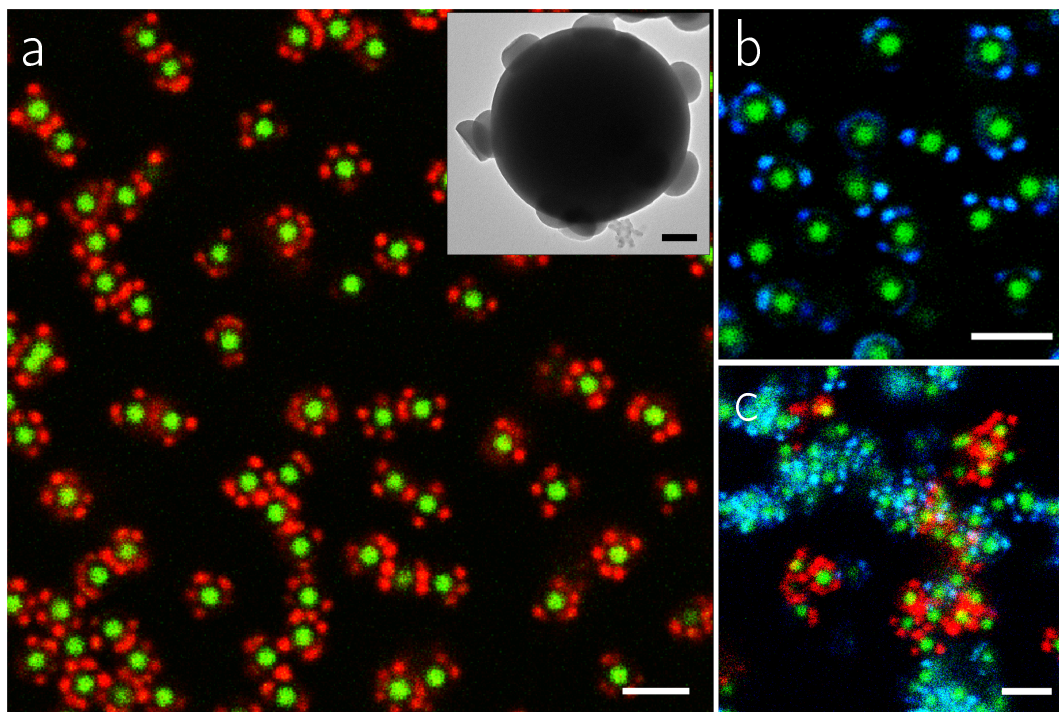

Figure 2: **Patchy silica particles with dye-labeled titania protrusions** fabricated by the anhydrous method with an octadecyltrimethoxysilane (OTMS) patterning. (a) Confocal micrograph of OTMS-patterned silica particles (core particle size 1085 ± 5 nm in ethanol (SLS)) with an FITC-labeled core (depicted in green) and RITC-labeled titania protrusions (depicted in red) in cyclohexyl chloride (CHC). Inset: TEM micrograph of one such particle. (b) Confocal micrograph of OTMS-patterned silica particles with an FITC-labeled core (depicted in green) and DEAC-SE-labeled titania protrusions (depicted in blue) in CHC. (c) Confocal micrograph of mixture of the particles used in (a) and (b). The scale bars denote $2 \, \mu$m and (inset) 200 nm.

Fluorescently-labeled silica protrusions

Van Blaaderen and Vrij incorporated a fluorescent dye derivative (fluorescein isothiocyanate,

8

FITC) into spherical silica particles by covalently coupling the dye to the silane coupling agent (SCA) 3-aminopropyltriethoxysilane (APTES), and allowing the conjugate to co-condense with the silica precursor.[89] FITC was incorporated selectively into silica protrusions using this method (SI§3/Fig. S5). Initially, however, the APTES-FITC conjugate facilitated silica growth on the antipatch, which was coated with MPTMS, most likely due to the positively charged amine group adsorbing also to the negatively charged antipatch. This excess silica growth reduced when the MPTMS grafting step was performed twice and the protrusions became well-defined. Nevertheless, a monolayer of attached FITC dye was still visible as a ring around the particles. This same issue occurred for an MPTMS grafting applied via the anhydrous route. A surface-patterning of SCA octadecyltrimethoxysilane (OTMS) instead of MTPMS, applied via the anhydrous route, did produce acceptable patch shapes and successfully prevented binding of APTES-dye conjugates, showing that OTMS molecules provide sufficient steric hindrance to shield the silica surface from dye-APTES conjugates forming siloxane bonds with the SCA coated surface. Surface-patterning with OTMS has the additional advantage that it creates a larger difference in hydrophobicity between the patch and the antipatch, increasing the chemical patchiness. However, the dispersability of OTMS-grafted particles in ethanol was low, and undesirable particle clustering takes place in the Stöber-like reaction mixture during protrusion growth, possibly affecting the protrusion shapes. Therefore, the dye-labelling method was further optimized as described below, by infiltrating titania protrusions with dye-SCA conjugate.

Fluorescently-labeled amorphous titania protrusions

Amorphous titania protrusions were grown onto MPTMS- and OTMS-patterned silica particles by hydrolysis and condensation of the titania precursor titanium IV butoxide (TBT).[48] In contrast to Bae and coworkers,[48] we did not observe a deterioration of the titania protrusion shape due to magnetic stirring. Occasionally, loose hemispherical protrusions were encountered in TEM images (see Fig. 2a, inset), most likely dislodged due to internal stresses caused by heating and/or densification by the electron beam.[90,91] Such an effect was pre-

9

viously observed by Demirörs *et al.* in silica-titania core-shell particles, where the titania core became movable upon annealing.[92] These amorphous titania protrusions were successfully labeled *post synthesis*, aided by the high microporosity of the amorphous and not fully condensed titania,[92] by infiltration with APTES-dye conjugate resulting in a covalent attachment of the dye rhodamine isothiocyanate (RITC) to the titania. These patchy particles were imaged *in situ* by confocal microscopy, where protrusions and cores were clearly distinguishable (Fig. 2a).

For future in-depth studies on the phase behaviour (e.g. gelation, see also section 'Self-assembly ... interactions' for more detail) of the patchy particles, it is interesting to have different dyes correspond to a specific type of surface ligand on the protrusion. The UV-excitable fluorescent dye 7-diethylaminocoumarin-3-carboxylic acid succinimidyl ester (DEAC-SE) was also incorporated into the titania protrusions (Fig. 2c). Trau *et al.* studied this dye previously at a silica surface.[93] DEAC-SE is amino-reactive and therefore was covalently linked to titania in the same way as the isothiocyanates FITC and RITC, i.e. via coupling to APTES and infiltration *post-synthesis*. With DEAC-SE emitting in the blue, these three dyes taken together allow to study mixtures of patchy particles (Fig. 2c).

Next we investigated whether the protrusions of the patchy particles could be characterized in-situ by the super-resolution microscopy techniques Stimulated Emission Depletion (STED) and Photo-Activated Localization Spectroscopy (PALM). A dye for PALM was selectively attached to the protrusions,[94,95] see SI§5 (Fig. S7). However, the improvement in resolution was modest compared to conventional confocal microscopy (Fig. S6) as the silica core and titania protrusions vary considerably in refractive index (n = 1.45 vs. n = 1.55[96]) such that these patchy particles cannot be completely index-matched. In future studies, it is therefore interesting to prepare all-titania patchy particles with a titania core and protrusions to benefit from increased resolution from STED or PALM.

Crystalline titania protrusions

For potential use in catalysis[97] or active matter,[23,97,98] it is of interest to convert the amor-

phous titania protrusions into crystalline polymorphs, as can be achieved by annealing. Non-labeled titania protrusions (Fig. S8) deformed in this process (Fig. S9a). In contrast, particles with titania protrusions that had been infiltrated with APTES-RITC were successfully annealed without any distortion of the protrusions (2 h at 500 °C, Fig. S9b). This difference in structural integrity is a result of the APTES forming an organosilica scaffolding inside the titania mesoporous structure, c.f. Demirörs *et al.* who observed that spherical amorphous and not fully condensed titania particles decrease as much as 40% in diameter at 650 °C due to the collapse of the porous structure,[92] while titania spheres infiltrated with silica shrink considerably less.[96]

To examine the crystallinity of the annealed dye-labeled titania protrusions, selected area electron diffraction (SAED) was performed (Fig. 3). Protrusions annealed at 500 °C diffracted the electron beam into rings, indicating the presence of a form of polycrystalline titania. Apparently, the silica does not intervene chemically at these temperatures and remains dispersed independently in between the crystallites, as already noted in ref. 96. Annealing for 8 h instead of 2 h at 500 °C produced slightly more pronounced rings. Protrusions annealed at 900 °C displayed diffraction spots rather than rings, indicating that these consisted of fewer crystalline domains with respect to the 274 nm area used to obtain the diffraction pattern. Annealing at 1100 °C produced diffraction spots only; this titania is predominantly monocrystalline. In short, higher annealing temperatures increase monocrystallinity in these titania protrusions, more so than longer annealing times do.

The electron diffraction patterns are in line with anatase titania (see SI§7), although the scarcity of diffraction spots in the SAED pattern of particles annealed at 1100 °C prevents conclusive identification of this titania polymorph. The monocrystallinity of these protrusions nevertheless showed in their faceting (Fig. 3e) and Bragg reflections in dark field TEM (Fig. S10).

Quantifying and modeling patch growth using TEM micrographs

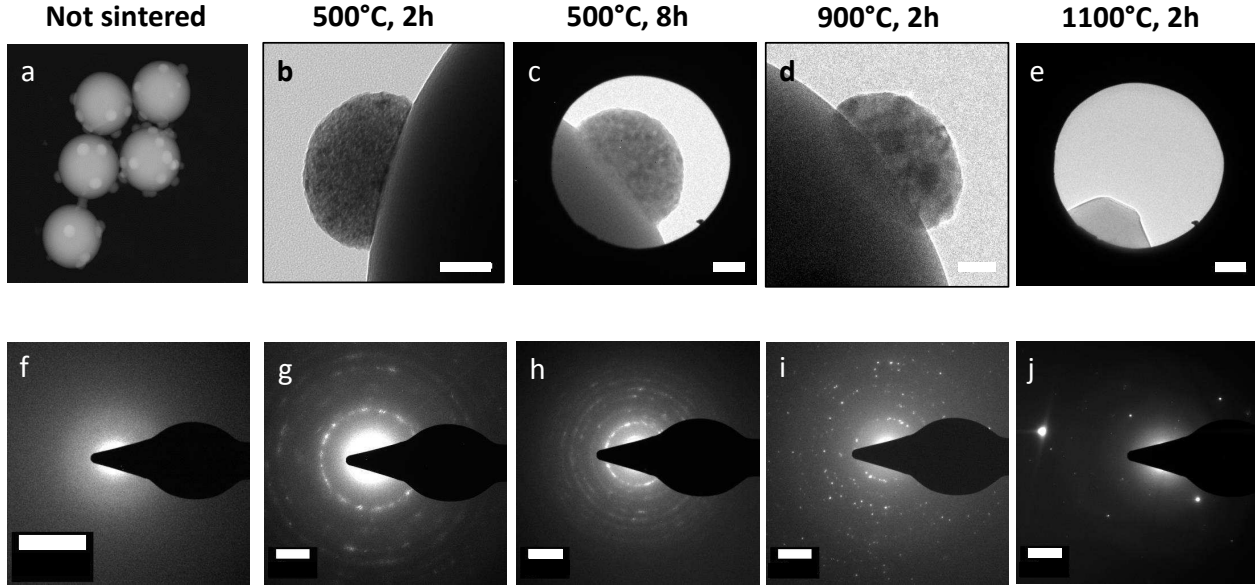To quantify the protrusion growth and evaluate quantitatively the effects of particle polydis-

Figure 3: **Crystalline titania protrusions.** Close-ups (top row) and electron diffraction patterns (bottom row) of patchy particles with APTES-RITC labeled titania protrusions annealed at various temperatures and annealing times: (a)/(f) no annealing; no diffraction rings or spots appear (b)/(g) 2 h at 500 °C; (c)/(h) 8 h at 500 °C; (d)/(i) 2 h at 900 °C; (e)/(j) 2 h at 1100 °C. Scale bars denote 50 nm.

persity, protrusion widths w and heights h were measured in TEM micrographs (Fig. 4). For both silica and titania protrusions, w increases as a function of average core particle diameter $\bar{\sigma}$. Note that here the error bars in the vertical direction denote not the measurement uncertainty but the standard deviation of w or h, that is, a polydispersity δ_w (δ_h) in the protrusion width (height). The protrusion width for particles of 411 nm with silica protrusions prepared via the annealing method ($w = 99$ nm, $\delta_w = 11$ nm) agrees well with that observed by Wang *et al.* for 415 nm particles ($w = 95$ nm, $\delta_w = 13$ nm).[47] Particles prepared by the annealing method[47] had larger widths w than those prepared by the anhydrous method, which is conform expectations since sintering broadens the contact areas.

We analyze the results in a simple model for the patch formation by assuming that patches result from size exclusion of the SCA from the contact areas in the crystal (Fig. 4c). In detail, the SCA molecule cannot reach the particles' surface from a location where the distance to the surface is longer than its stretched length d. The volume containing such

positions around a particle of radius R is a shell of radius $R+d$. The patch is formed by the intersection of the shells (patch radius $w/2$ indicated in green), yielding a patch width w of:

$$w = 2R\cos^{-1}\left(\frac{R}{R+d}\right) \tag{1}$$

Based on atom-atom bond lengths and angles[99] the maximum length of a stretched MPTMS molecule is 1.9 nm. The experimental values for silica patch widths (without sintering), however, are better described by the curves of predicted patch sizes for $d = 4$ nm, see Fig. 4a. A plausible reason is that the SCA molecules form oligomers before attaching to the surface, resulting in a larger effective size d. In addition, surface roughness is not taken into account in this simple model. OTMS molecules (of maximum stretched length 3.3 nm) are larger than MPTMS molecules and this explains why titania protrusion widths correlated best with an even larger effective size $d = 12$ nm (Fig. 4b).

Protrusion heights h for silica patches remained nearly constant with core particle diameter (Fig. 4a), whereas an increase was expected (see SI§7 for a calculation). For titania protrusions, h did increase with particle diameter. This difference can not be attributed to a larger amount of precursor [we added 9 μmol TES versus only 0.3 μmol TBT per milligram silica particles]. We tentatively attribute this discrepancy to TES hydrolysis and condensation in base-catalyzed solutions continuing beyond the two hours of reaction time.[100–102] Despite the addition of the TES happening over 11 h, possibly not all added TES condensed over the subsequent 2 h of reaction time.

Number distributions of patches/protrusions per particle: theory and experiment

The number of protrusions on a patchy particle can be determined accurately using electron tomography, as we performed in Fig. 1b. However, this technique is too laborious for a large number of particles. When cores and protrusions are labeled with different dyes, confocal microscopy becomes a powerful tool to study large numbers of patchy particles. We demonstrate here that confocal microscopy can be used (1) to reconstruct dispersions
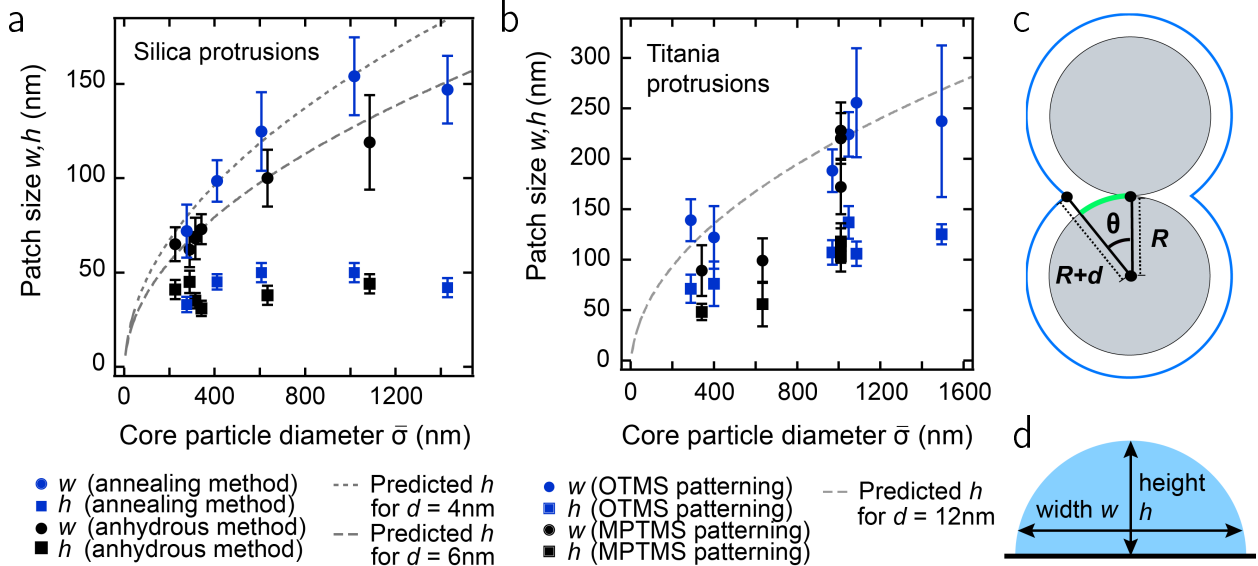
Figure 4: **Protrusion dimensions: widths and heights.** (a) Average patch widths w (circles) and heights h (squares) as a function of core particle diameter $\bar{\sigma}$ for patchy particles grown via the annealing method (blue) and via the anhydrous method (black). The patch sizes of the 'annealed' (blue) series are plotted against the particle diameter as measured after annealing, which is responsible for the slight offset in $\bar{\sigma}$. Error bars for the average particle diameter are generally smaller than the symbol size. Error bars in the vertical direction are standard deviations of the patch size measurements, i.e. a 'polydispersity' in the patch size. Dashed lines are fits to Eq 1 for $d = 4$ nm and $d = 6$ nm. (b) Average patch size of titania protrusions[48] as a function of $\bar{\sigma}$. Blue symbols indicate an OTMS patterning, and black symbols an MPTMS patterning. The dashed line is a fit to Eq 1 for $d = 12$ nm. (c) Schematic indicating the parameters used to predict protrusion widths. R is the particle radius, d is the size of the grafting molecule, and θ is opening angle of the patch. (d) Schematic indicating how patch width w and patch heights h were measured.

of patchy particles to observe their 3D structure[81] and (2) to extract meaningful data such as the distribution of protrusions per particle and the symmetry of the patches around each core, reflecting the local symmetry inside the colloidal crystal from which they originated.

Supplementary video SV4 shows a confocal z-stack of patchy particles (silica core particles of diameter 1085 nm and 1% polydispersity, with titania protrusions) in dodecanol (n = 1.44 at 20 °C, nearly matching silica), which we refer to as sample A. Figure 5a shows a single slice from this stack. The frames of the 3D stack can be split into images with only cores (Fig. 5b) or only protrusions (Fig. 5c) on account of the different labelings. A tracking algorithm was developed with which the positions of particle cores and protrusions within the stack
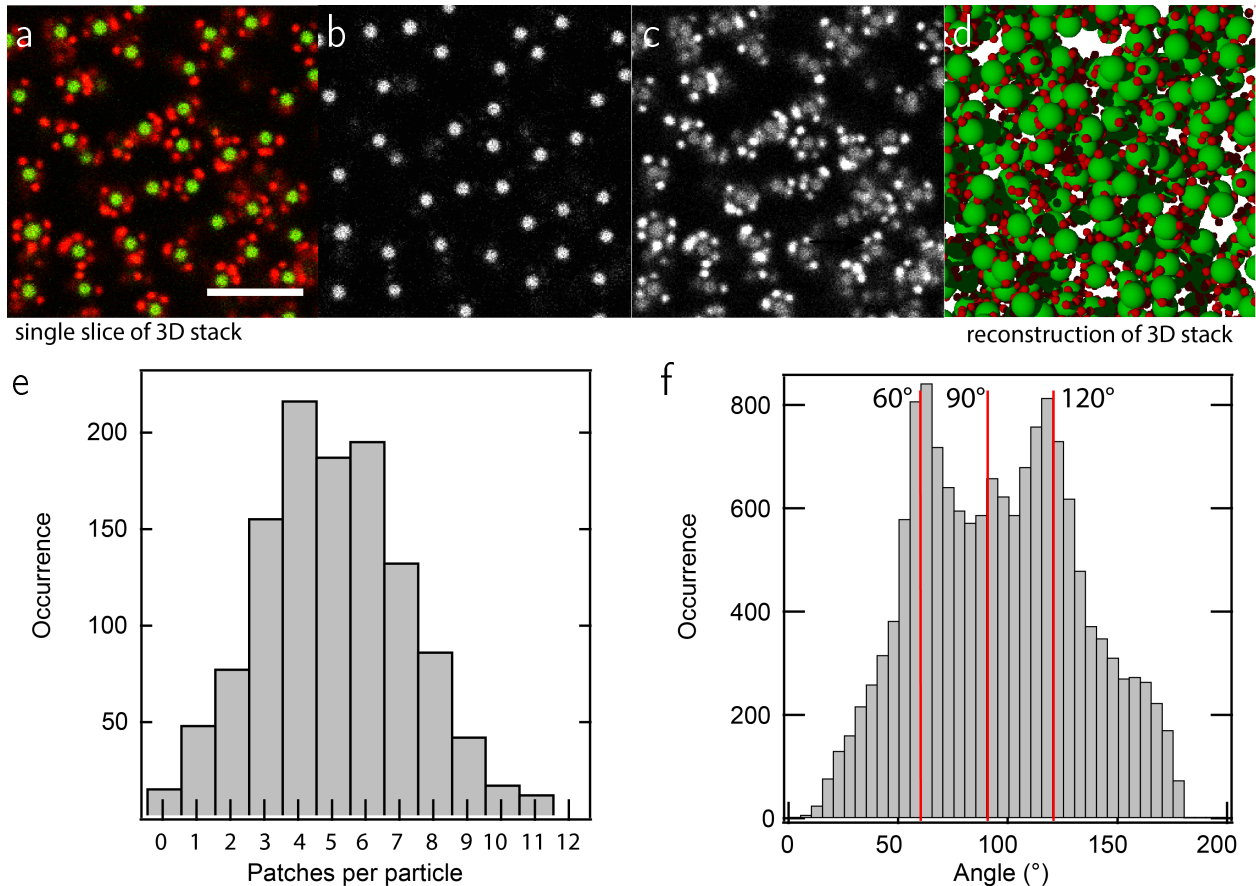
single slice of 3D stack

reconstruction of 3D stack

Figure 5: **Tracking and particle fitting from a 3D confocal data set, and experimental patch number distributions.** (a) Single slice in a 3D confocal stack of patchy silica particles with dye-labeled titania protrusions in dodecanol. Scale bar denotes $4\,\mu$m. The full stack is displayed in Supplementary Video SV4. FITC-labeled cores are displayed in green and RITC-labeled protrusions in red. (b,c) The same image as in (a) split by the imaging channels, resulting in (b) mostly cores and (c) only protrusions. There is a slight bleeding-through of the FITC into the RITC channel. (d) Computer-rendered reconstruction of the dispersion, obtained by smoothing, thresholding and tracking the image frames split by channel as in b,c. This image displays all core particles (green) and patches (red). (e) Patch number distributions obtained from the particle tracking the dispersion of patchy particles (Fig. S11). (f) Histogram of the angles between all protrusions on each particle, for the same dispersion as in (e).

were determined, and a digital directory of these positions created. By attributing to the core and the protrusions radii *d1* and *d2*, known from TEM measurements, a computer-rendered reconstruction of the dispersion was then obtained. The algorithm was first tested on a sparse sample of patchy particles (Fig. S11a,b) and subsequently used to track and reconstruct sample *A* (Fig. 5d, and full figure in Fig. S11c).
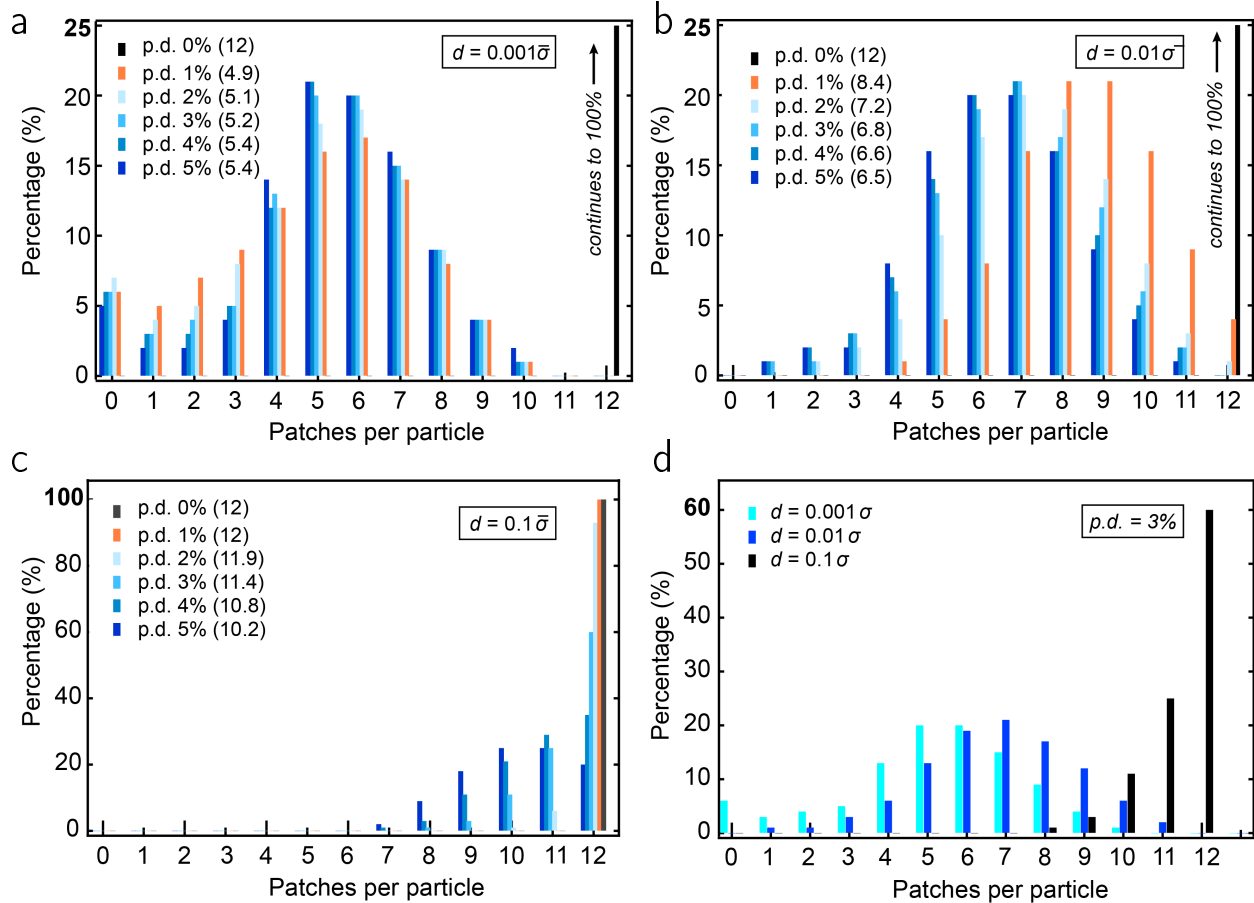
15

Figure 6: **Patch number distributions as calculated by simulations** for particles of $p.d. = 0\,\% \text{-} 5\,\%$ and cut-off distance (a) $d = 0.001\,\bar{\sigma}$, (b) $d = 0.01\,\bar{\sigma}$ and (c) $d = 0.1\,\bar{\sigma}$. The vertical axis is discontinued at $25\,\%$ for clarity in panels (a) and (b). In the legends, the average number of patches per particle is indicated in brackets for each distribution. (d) Patch number distributions as calculated by NPT simulations for particles of $p.d. = 3\,\%$, comparing the distributions for three different cut-off distances d.

The average number of protrusions per particle follows immediately from the number of cores and protrusions found by the tracking algorithm. For sample A, tracking revealed 1194 cores and 5994 patches, or an average patch number of 5.0. To establish how the protrusions are distributed over the core particles, each protrusion was assigned to its closest core. A cut-off distance of $1.5\bar{\sigma}/2$ for the maximum allowed distance of a protrusion to a core was also determined (Fig. S11d). Subsequently, the number of protrusions was counted for each core, yielding the histogram in Fig. 5e for sample A. The histrogram reveals a distribution centered around 5 protrusions per particle, with an FWHM of ≈ 2 protrusions/particle, a

point we will come back to later. The angles between any two protrusions on each core particle were also extracted, yielding the histogram in (Fig. 5f). The distribution displays clear peaks at 60 °, 90 °, 120 °, which correspond well with the bond angles in an FCC colloidal crystal. Most likely the colloidal crystal also contained glassy areas, since the peaks in the bond angle distribution are broad. The resolution of the distribution also does not allow to discern whether there is a contribution of hexagonal close packed (HCP) order, which would be visible as additional peaks or shoulder peaks at 108 ° and 146 °. Nevertheless, these data show that the protrusions are indeed located at the points of contact in a close-packed colloidal crystal, even though in TEM images this order is difficult to discern due to the low average number of protrusions per particle (5.0).

To further put these experimental results into perspective, patch number distributions were predicted by simulations (see *Methods* for computational details). The influence of two particle characteristics were examined: the size polydispersity of the core particle, denoted *p.d.*, and the maximum 'allowed' separation between the particle surfaces that still results in patch formation, called the cut-off distance d. Fig. 6a shows simulated patch number distributions for a fixed cut-off distance of 0.1% of the average core particle diameter $\bar{\sigma}$ and varying *p.d.* For a purely monodisperse system, all particles possess twelve patches (black graph), as expected in a close-packed crystal. For higher *p.d.*, the patch number distribution quickly drops to lower average patch numbers of around 5 patches per particle. This finding is in agreement with the experimental results in Fig. 5, and explains why in general the presented synthesis method will not yield 'perfect' particles with 12 patches. For larger cut-off distances d, the decrease in average patch number with increasing *p.d.* is smaller (Figs. 6a-c). This becomes even better visible in Fig. 6d, where the patch number distributions are displayed for a fixed *p.d.* (3%) but varying d. The number of patches per particle shifts to higher values for increasing cut-off distances d, in accordance with our model in Fig. 4.

We compare our experimental results to these simulations. We estimate the experimental

cut-off distance for the core particles of the sample in Fig. 5 to be $d = 0.003\,\bar{\sigma}$ - $d = 0.011\,\bar{\sigma}$ (since $\bar{\sigma} = 1085\,\mathrm{nm}$ and $d = 3\,\mathrm{nm}$ - $12\,\mathrm{nm}$ based on OTMS stretched length of $3.3\,\mathrm{nm}$ and the fitted $d = 12\,\mathrm{nm}$ in Fig. 4b). For $p.d. = 1\%$, the simulations predict a patch number distribution centered around 6 patches per particle (with an average of 4.9) for $d = 0.001\bar{\sigma}$, and a distribution centered around 8-9 patches per particle (with an average of 8.4) for $d = 0.01\bar{\sigma}$ (Figs. 6a-b). That is, the experimentally observed distribution with an average of 5.0 patches per particle is in agreement with the expected patch numbers based on the simulations, but only when the stretched length of the polymer is taken as the cut-off distance rather than their fitted effective size. An explanation for the discrepancy is that domain walls, point defects and cracks were not taken into account in the simulations. On the experimental side, small patches (e.g. with a cross section smaller than one pixel) may not be recorded in the confocal microscope or not counted in the tracking algorithm. The possibility that some titania grows beyond the edges of the patch, hence increasing the fitted effective size of the grafting molecule, can not be excluded either.

Self-assembly of patchy particles via solvophobic interactions

Patchy silica particles with titania protrusions can potentially sustain patch-patch interactions. In low-polar media, the OTMS chains are solvated and provide steric stabilization, and in addition cause the antipatches to repel each other via a steric interaction. The titania protrusions, on the other hand, do not have a steric stabilization to counteract the van der Waals attractions among them, and this possibly creates patch-patch attractions. In addition, the particles' surfaces may carry charge from (remaining) terminal OH groups at the patches and protrusions, causing charge-related attractions or repulsions. Here, we manipulated the interactions between patchy particles (with titania protrusions and OTMS patterning on the antipatch) by dispersing them in cyclohexyl chloride (CHC) and 1,2-dichloroethane (DCE). The potential patch-patch interactions are based on van der Waals interactions, hence irreversible in character, and therefore these particles are expected to form gels rather than crystalline structures upon self-assembly via such interactions. Moreover, the complex col-

loids presented here possess a comparatively wide distribution of the number of patches per particle, hence even in the case of reversible interactions, gel structures would be expected for this particular system of patchy particles.
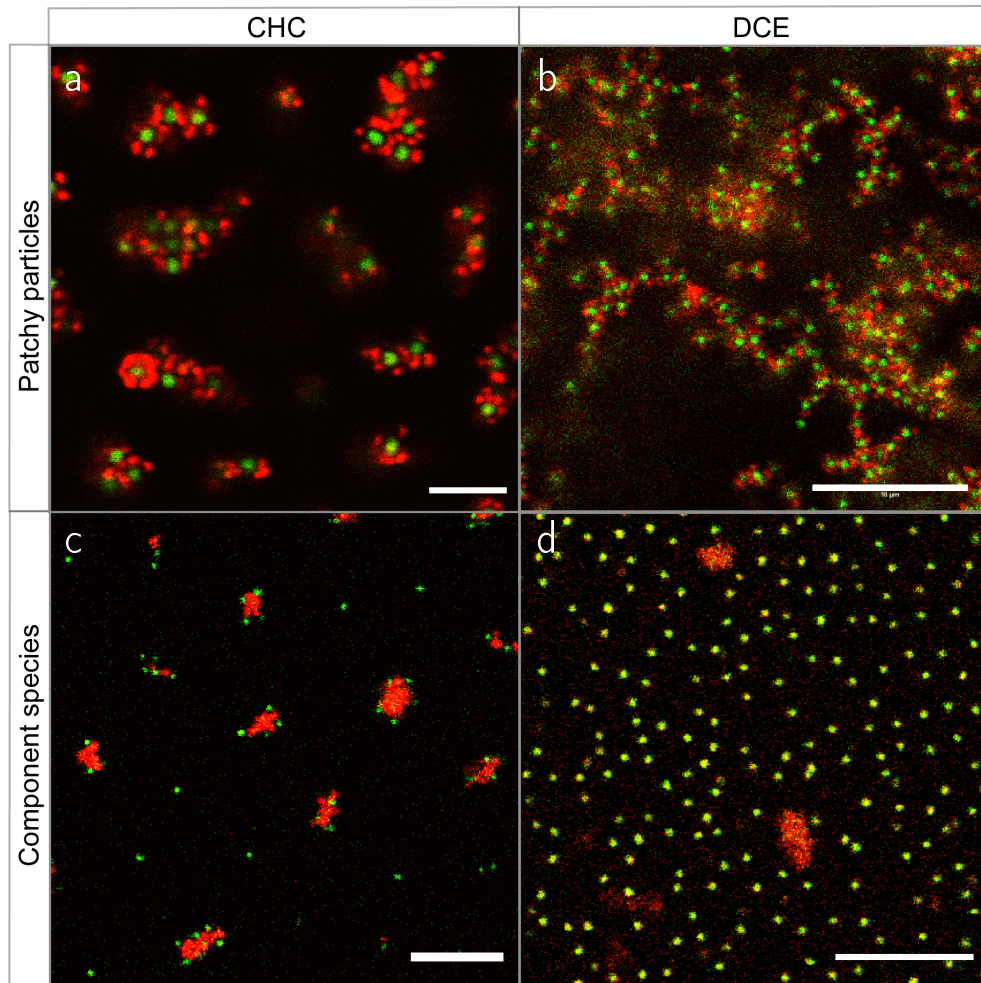

Figure 7: **Patchy particles and component species in CHC and DCE.** (a) Patchy particles (silica core of $1.0\,\mu$m, with OTMS patterning and RITC-labeled titania protrusions) dispersed in (a) CHC and (b) DCE, after turning the sample upside down for confocal imaging. (c) OTMS-grafted silica and RITC-labeled titania in CHC. The surface charge was negative on the silica and positive on the titania. (d) OTMS-grafted silica and RITC-labeled titania in DCE. The surface charge was positive both on the silica and the titania. A gaussian filter was applied to all images to reduce noise.

Both in CHC and in DCE, percolating open gel phases were indeed observed for these patchy particles (see Fig. 7a,b and Supplementary Videos SV5,6). To investigate the nature of the inter-particle interactions, we mixed dispersions of (non-patchy) OTMS-grafted

silica particles with dispersions of RITC-infiltrated titania particles. In deionized CHC, the OTMS-grafted silica particles formed a hexagonal long-ranged crystal[103,104] indicating a strong electrostatic repulsion, while RITC-labeled titania particles aggregated. When mixed, the silica particles adhered to the titania clusters in this medium (Fig. 7c and Supplementary Video SV7). This observation implies that in dispersions of patchy particles *in CHC*, the protrusions stick to the antipatch (and likely also to other titania protrusions, that is, the particles behave only partially as 'inverse patchy particles'[15,75–77]). In DCE ,on the other hand, the titania particles also formed large aggregates, but the two types of particles did not adhere to each other (Fig. 7d and Supplementary Video SV8). It is therefore likely that *in DCE* the protrusions adhere exclusively to other protrusions; a patch-patch interaction.

To gain further insight into the charge interactions in the systems, the electrophoretic mobility of titania particles and OTMS-grafted silica particles were measured in both these low-polar media using laser Doppler electrophoresis. Since RITC absorbs the laser wavelength (633 nm), non-labeled titania was used as an indication of the sign and order of magnitude of the charge. While the titania particles were positively charged in both DCE and CHC, the OTMS-silica particles were negatively charged in CHC and positively charged in DCE (SI§9/Fig. S12). Therefore, it is likely that *in CHC* the (positively charged) titania protrusions stick to the (negatively charged) OTMS-silica cores. In contrast, *in DCE* all constituents are positively charged, and since the particles form a network, most likely the titania protrusions adhere to other protrusions. Such a patch-patch attraction could have a partially solvophobic character given the absence of alkane chains, and van der Waals attraction will certainly also contribute given the dielectric constant mismatch.

The gel structure in DCE (as well as the one in dodecanol, Supplementary video SV4 and Fig. S13) illustrates the prediction by Bianchi *et al.* in ref. 28: "it is foreseeable that, with small $\langle M \rangle$ patchy particles," (here $\langle M \rangle = 5.0$) "disordered states in which particles are interconnected in a persistent gel network can be reached at low T without encountering phase separation."

SUMMARY

We prepared patchy particles with silica and titania protrusions by extending upon the works of Wang *et al.*[47] and Bae *et al.*[48] For the case of silica protrusions, we made the following advancements. Through an anhydrous grafting method of the silane coupling agents used to cover the exposed silica surfaces, we were able to eliminate the need for a temperature-induced annealing step in the synthesis route. A fluorescent dye was incorporated into the protrusions via the method of van Blaaderen *et al.*,[89] for which it was important to use a patterning of the silane coupling agent OTMS to cover free silica surfaces and to prevent binding of the dye conjugate to the antipatch. Electron micrographs were used to examine how the size of the protrusions depends on core particle size and synthesis route. A simple model was used to estimate how the diameter of the protrusions was dependent on the core particle diameter in a way consistent with size exclusion of (oligomers of) the grafting molecule from the contact areas. We also extended the synthesis method to silica rods, which resulted in fluted rodlike particles with up to six wing-shaped protrusions along the length of the rods.

The following advancements were made for the case of titania protrusions. Titania protrusions were covalently labeled *post synthesis* with various fluorescent dyes (FITC, RITC and DEAC-SE) by infiltration of the porous titania with dye-APTES conjugate, rendering the particles suitable for confocal microscopy. DEAC-SE is a blue-emitting dye which was used for the first time here to label colloidal particles for confocal microscopy. The protrusions were also successfully labeled with the rhodamine derivative Cage 552 and imaged by the super-resolution technique PALM. True nanoscopy resolutions as obtainable through STED confocal microcopy were not achieved, most likely because of the negative effect of the scattering titania patches on the point spread function.

Patchy particles with titania protrusions infiltrated with rhodamine-APTES were annealed at temperatures up to $900\,^{\circ}\mathrm{C}$, which converted the protrusions to anatase titania (most likely within a silica matrix) with excellent preservation of the protrusion shapes. The

domain sizes of crystallites increased with annealing time and temperature. These findings are potentially useful for catalytic processes and self-propelling particles.

We performed simulations in which randomly distributed polydisperse particles on face-centered cubic colloidal crystal lattices were compressed, to simulate our experimental procedure. In these simulations, size polydispersity and maximum particle-to-particle separation d (representing the grafting molecule size, but also kinetic factors such as the probability to diffuse into small crevices) were taken into account. As expected, a small polydispersity (1%) already had a large influence on the average number of patches per particle: the median patch number shifted from 12 for perfectly monodisperse particles to 6 for the case of $d = 0.001\bar{\sigma}$. Fluorescent labeling enabled us to experimentally determine the number of patches/protrusions per particle in our samples in a much more facile way than by electron tomography, namely by analyzing 3D confocal z-stacks. A particle tracking and bond order analysis algorithm was used to render the structure of the particle dispersions and extract patch number distributions and the local symmetries around each particle on which the patches formed. For a sample of core particle dispersity 1%, an average patch number of 5.0 was found (1194 counted cores). The patch number distribution was centered around 5 patches per particle, close to the prediction from simulations for a cut-off distance of $0.001\bar{\sigma}$ (distribution centered around 6 patches per particle). The angles between the protrusions agreed with the bond angles of an FCC lattice.

According to the simulations, a particle core polydispersity below 0.5% is required to approach 12 patches per particle in future studies (for silane-coupling agents in nm size range and colloids of several hundred nm in diameter). Alternatively, a cut-off distance d close to $0.1\bar{\sigma}$ may be used, however, experimentally, kinetic effects may prevent longer molecules from diffusing into the colloidal crystal. A third route to increase the number or patches could be the use of more deformable particles, such as silica shells.[105,106] Centrifugation techniques such as in refs. 107–109 may be applied in future research to separate particles of different patch numbers. In a glassy system, the volume fraction and number of contacts

among colloids may even be slightly higher than in a colloidal crystal,[110] so colloidal glasses could be used to increase the patch number and/or to obtain patchy particles with more than twelve patches. However, the distribution of the patches on the particles would be much more random, making it not possible to self-assemble into more regular, crystalline arrangements.

Finally, we showed that patchy silica particles with titania protrusions form gel structures in the low-polar solvents DCE and CHC. The steric stabilization provided by the SCA grafting prevents the silica surfaces/core particles from adhering to each other, leaving the possibility that the patches adhere to other patches or to the antipatch. The nature of the inter-particle interactions was further investigated by mixing silica spheres and dye-labeled titania and OTMS-grafted silica spheres separately in CHC and in DCE. We found that both types of particles are positively charged in DCE, while in CHC the OTMS-grafted silica was negatively charged and the titania positively charged. Therefore we posit that in CHC protrusions adhere to the antipatch or to other protrusions due to the absence of a hydrophobic grafting and sufficient charge stabilization, and in DCE to other protrusions only (a patch-patch interaction).

In short, we developed a system of patchy particles with protrusions that can be imaged and characterized by confocal microscopy. Towards this goal, the particles had a fluorescent dye incorporated into or selectively attached to the protrusions. The infiltration with SCA also rendered the titania protrusions stable against annealing, which may be important for applications in catalysis and active matter. We exploited the fluorescently labeled patchy particles to obtain the dispersion structure in 3D from confocal z-stacks, and to extract data on the numbers and symmetries of protrusions per particle, in this way being able study much larger numbers of particles than via electron tomography. The experimental data were compared to simulations predicting the number of contact points in a colloidal crystal as a function of core particle polydispersity $p.d.$ and the cut-off distance for patch formation d, and showed good agreement. Finally, we illustrated in several preliminary examples that

it is possible to quantitatively investigate, using confocal microscopy, the self-assembly of these patchy particles in low-polar index-matching media. Open gel-like structures were observed in several cases, where attractions between patches on the particles were present next to charge and steric repulsions between other parts of the particles of which each role in the structures being formed warrants further research. From these preliminary self-assembly studies, it is clear that a broad range of shorter and longer ranged repulsions between different parts of the particles can be present next to attractions between the patches (and possibly other parts of the particles). This allows a broad range of conditions that can be probed by exploiting differences in solvents on the charging behavior and ionic strength. It is also clear that the methodology used can be extended to amorphous packing of the particles used, giving almost identical patch numbers, but with a much less regular distribution over the particle surface, allowing the role of symmetry of the patch distribution to be investigated as well.

METHODS

Materials

Solvents used were ethanol (absolute, Merck), ethylene glycol ($\geq$99.5 wt.%, Fluka), acetone (pro analysis, Merck) and toluene ($\geq$99.5 wt.%, Sigma Aldrich). Water was deionized with a MilliQ system (Millipore Corporation) and had a resistivity of at least $18.2\,\mathrm{M\Omega cm}$. The catalysts aqueous ammonia ($\sim$25 wt.%) and n-butylamine (99.5 wt.%) were purchased from Sigma Aldrich. Silane coupling agents used were: (3-aminopropyl)triethoxysilane (APTES, $\geq$98%, Sigma Aldrich), 3-methacryloxypropyltrimethoxysilane (MPTMS, $\geq$98 wt.%, Sigma Aldrich, is also known as 'TPM' for '3-(trimethoxysilyl)propyl methacrylate') and octadecyl-trimethoxysilane (OTMS, 95% [85% n-isomer], ABCR GmbH & Co via Gelest, Inc.). Precursors tetraethylorthosilicate (TES, 98 wt.%) and titanium (IV) butoxide (TBT, 97 wt.%)

were obtained from Aldrich. The dyes fluoresceine isothiocyanate (FITC, $\geq$90 wt.% (HPLC)) and rhodamine B isothiocyanate (RITC, mixed isomers) were ordered from Sigma Aldrich, while 7-diethylaminocoumarin-3-carboxylic acid succinimidyl ester (DEAC-SE) was purchased from Thermo Fisher. All chemicals were used as received without further purification.

Sintering for the synthesis of silica particles with silica protrusions was carried out in a Carbolite AAF ashing furnace, while a similar Carbolite oven with type 301 controller was employed to anneal patchy particles with titania protrusions. For high power sonication (to break up and redisperse sintered colloidal crystals) we employed a Vibra-Cell ultrasonic processor (750 W) from Sonics & Materials, Inc. Syringe pumps applied in the silica protrusion growth step were from KD Scientific, models KDS-410 (single syringe pump) and KDS-200-CE (double syringe pump). IKA RH Basic stirrers were used for magnetic stirring during silica growth.

Synthesis of silica particles with silica protrusions

Fluorescently-labeled silica seeds were prepared by the method introduced by Van Blaaderen and Vrij.[89,111] A non-fluorescent silica shell was grown onto the seed particles according to the continuous growth method by Giesche,[112] which is a modification of the method by Bogush et al.[113] Colloidal crystals were then prepared from the silica colloids as follows. Particles in the size range of 0.20 - 1.1 μm and of polydispersity $\leq$6% were dispersed in ethanol at volume fractions 1-5%. They were allowed to sediment in 20 mL vial with a flat bottom and form a flat, close-packed (FCC and/or HCP) crystal.[114–116] After crystal formation, the vial was opened and the ethanol was left to evaporate at room temperature.

To pattern the particles' surfaces with MPTMS,[47] pieces of crystal were placed in a ceramic cup inside a calcination furnace. The particles were annealed at 750 °C for five hours with one hour heat-up and cooling-down time. To coat the free surfaces of the particles, 50 mg of annealed colloidal crystal were placed into a reaction mixture of 40 mL ethanol, 1.5 g H_2O, 0.50 mL silane coupling agent MPTMS and 1.0 mL aqueous ammonia. The mixture

was left for 24 hours in quiescent condition. The colloidal crystal was then washed five times with ethanol to remove non-reacted silane coupling agent. For a *double* MPTMS grafting, the crystal was dried under a stream of nitrogen, and the same coating step repeated The crystal was broken up into individual particles in ethanol using an ultrasonic processor (at 25% amplitude for 0.5 h and with pulses of 5 s at 1 s intervals). Crystals larger than a few millimeters in diameter were broken up into smaller pieces with a spatula prior to sonication, as we found that such large crystals did not break up through sonication within a reasonable time span (2 h).

To grow silica protrusions onto MPTMS-patterned particles, we used the method of Wang *et al.*,[47] however, all volumes were five times smaller: to 8.0 mL of a dispersion of patterned silica particles were added 1.00 g water and 0.20 mL aqueous ammonia. The silica content was not adjusted for particle size, but kept at 0.50 g/L. A TES solution (8.0 μL TES in 8.0 mL ethanol) was added under magnetic stirring at a rate of 0.72 mL/h, using a syringe pump. For micron-sized particles, the total amount of TES solution added was increased to 16.0 mL, still added at a rate of 0.72 mL/h. In one experiment, the influence of extended protrusion growth on MPTMS-patterned particles was studied. In this study, a total volume of 24 μL TES in 24.0 mL ethanol was added under magnetic stirring (still at a rate of 0.72 mL/h). After 17.3 mL of precursor solution had been added, 0.30 mL of aqueous ammonia was added to compensate for the dilution of the ammonia concentration by the added TES/ethanol mixture.

We found that the annealing step can be circumvented by carrying out the grafting step in an apolar solvent such as toluene; we call this grafting method the 'anhydrous' route. A dried colloidal silica crystal was not found to redisperse when placed in toluene, probably as a result of the hydrophilicity of the particle surface. We typically placed ∼20 mg crystal in a reaction mixture[117,118] of toluene (10.0 mL), butylamine (1.0 mL) and silane coupling agent MPTMS or OTMS (1.0 mL). The butylamine acts as a catalyst, analogously to ammonia in the Stöber-like method. The colloidal crystal was left in the reaction mixture for 24 h. The

crystal was washed once with toluene, and placed in an oven at 100 °C for one hour to ensure complete condensation of the silane coupling agent with the silica surface. Two additional washing steps with toluene and three with ethanol followed. Finally, the crystal was placed in ethanol and broken up by sonication with an ultrasonic processor (0.5 h at an amplitude of 25% and with pulses of 5 s at 1 s intervals).

Fluorescently labeled silica protrusions

To grow silica protrusions with a fluorescent dye incorporated, either a double MPTMS grafting via a Stöber-like method or an OTMS-grafting via the 'anhydrous' route was needed, in order to prevent silica growth on the antipatch region. The crystal was dried under nitrogen, weighed, and broken up into single particles by sonication in ethanol with the high-power ultrasonic processor. A dispersion of 0.50 mg/mL surface-patterned particles in ethanol was then prepared. To 1.5 mL dispersion we slowly added two solutions, both at a rate of 67.5 μL/min: 1.5 mL of a solution of TES and 1.5 mL of a solution of dye. The TES solution consisted of 2.0 μL/mL TES in ethanol. The dye solution was prepared using a recipe based on refs. 89 and 111, by first letting 5.0 mg APTES and 5.0 mg FITC react in 312 μL ethanol in the dark for 8 hours, and then diluting 15.0 μL of this solution in 10.0 mL ethanol. These two solutions were added to the reaction mixture with a syringe pump from separate syringes, and under magnetic stirring. After all TES solution and dye solution had been mixed in, the reaction mixture was left to stir for five more hours, and the particles were washed with ethanol until no coloration of the supernatant was observed.

Growth of titania protrusions

Titania protrusions were grown according to the method by Bae *et al.*[119] We prepared a solution of 200 μL TBT in 30 mL of ethylene glycol and stirred it for 12 h - 24 h. Dry OTMS-patterned (anhydrous route) particles (1.12 ± 0.01 μm) were dispersed in acetone at a concentration of 2 mg/mL. To 40 mL of this dispersion, we added 100 μL water (needed for

hydrolysis of the TBT). Under magnetic stirring, we then added 0.5 mL of the TBT solution. The reaction mixture was left stirring overnight and the patchy particles were collected by centrifugation and washing with ethanol.

Fluorescent labeling of titania protrusions by infiltration with APTES-dye conjugates, and annealing

The titania protrusions were successfully labeled with a fluorescent dye *post synthesis*. A solution of RITC (or FITC, or DEAC-SE) conjugated to APTES was first prepared as follows: to 20 mg RITC (or FITC, or DEAC-SE) were added 1 g (1.27 mL) ethanol and 20 μL APTES, after which the solution was stirred overnight. To 10 mL of a dispersion of the silica particles with titania protrusions, 100 μL aqueous ammonia and 40 μL dye solution were added. The APTES-RITC (or APTES-FITC, or APTES-[DEAC-SE]) conjugate molecules can penetrate the porous titania and react with the surface OH groups, as already shown before by Demirörs *et al.*[96] The dispersion was shaken for two hours. The residual dye was washed away by centrifuging and replacing the supernatant with fresh ethanol until not visibly colored with dye anymore (>3 washing steps).

Some of the final particles were annealed with the objective of converting the amorphous titania protrusions into crystalline titania. Particles were dried in a ceramic cup and placed in a calcination furnace under ambient conditions. The furnace was heated to the desired temperature (500 °C, 900 °C or 1100 °C) at a heating rate of 9 °C/min. After annealing for the desired time, the furnace was left to cool by itself. The ceramic cup was placed in a beaker with 40 mL of ethanol. The beaker was placed in a sonication bath to collect the annealed particles in the form of a colloidal dispersion in ethanol.

Characterization of particle and protrusion sizes by Transmission Electron Microscopy (TEM), and electron tomography

The shape of patchy particles was examined by transmission electron microscopy (TEM) with a FEI Tecnai 10 or Tecnai 12 microscope, at respective acceleration voltages of 100 kV and 120 kV. High-Resolution Transmission Electron Microscopy (HR-TEM) and Selected Area Electron Diffraction (SAED) were performed on a Tecnai 20 FEG (FEI) at an acceleration voltage of 200 kV. Home-made TEM grids were used as sample holders (preparation: cf. ref. 120, on G200-Cu grids by Electron Microscopy Sciences). The particles were dropcast onto the grids and dried from ethanol. Scanning electron microscopy (SEM) images were obtained utilizing a table-top Phenom or a Nova Nanolab 600 (FEI).

Particle and patch sizes were obtained from TEM images via the software program *iTEM* (version 5.0, Olympus Soft-Imaging Solutions Corp.). As uncertainty in the particle diameter, we used the standard deviation of at least ten diameter measurements on a single particle, while the standard deviation of measurements on different particles was used as the polydispersity. Patch widths and heights were estimated by drawing line segments tangentially and orthogonally (respectively) to the core particle through the patch projection. Each patch size measurement was averaged over at least twenty counts of different patches. The standard deviation of these measurements was used as a 'polydispersity' of the patch size.

For some particles we determined the 3D shape by electron tomography (see ref. 121, 122). Electron tomography is a technique with which the 3D morphology of an object can be determined by repeated TEM imaging and sample rotations. All images are Fourier transformed and combined. The Projection Theorem states that the 2D Fourier transform of a 2D image is equal to a 2D slice through a 3D Fourier transform of a 3D image.[123–125] A 3D inverse Fourier transform of the combined slices therefore yields a 3D image of the particle surface. The quality of the reconstruction depends on the total range of tilt angles over which the 2D images were acquired. Here, the tilt angle ranged between $-60°$ and

+60 $^\circ$ recorded at intervals of 1 $^\circ$ - 2 $^\circ$.

Zeta potential measurements

Zeta potential measurements were performed on a Malvern ZetaSizer Nano ZS machine, which measures mobilities by means of laser Doppler micro-electrophoresis. Since the measurements involved inorganic sovents, a Malvern 'dip cell' probe and a fused glass cuvette were empoyed. Mobility measurements consisted of 50-100 runs at a temperature of 25°C and a voltage of 40 V. For data acquisition, we used Malvern Zeta Sizer software version 5.1.

Characterization by confocal microscopy

Confocal images were recorded on a Leica SP8 confocal microscope with a 100x oil immersion objective (Leica HCX Plan Apo STED Orange, designed for the purpose of STED microscopy, NA $= 1.4$). This confocal microscope was fitted with a white light fiber laser; the wavelengths 495 nm and 543 nm were selected to excite FITC and RITC dye, respectively. The microscope was equipped with two types of detectors: photomultiplier tubes (PMT) and hybrid detectors (HyD) developed by Leica. HyD detectors combine a traditional PMT with an avalanche photo diode (APD), resulting in a higher sensitivity and signal-to-noise ratio for these detectors. Fluorescent signals from the dyes were recorded on such HyD detectors. For imaging of particles with DEAC-SE dye, we used a similar microscope set-up equipped with a 405 nm diode laser. Samples were either prepared by filling a borosilicate capillary (VitroCom no. 5010 or no. 5012, $n = 1.474$ at 589.3 nm) or by building a sample cell from cover slips (Menzel Gläzer, no.1) as in ref. 126. The capillaries were sealed with Norland Optical Adhesive no.68, which was cured under UV light (~350 nm). Immersion oil (Leica, Type F, $n = 1.52$) was used between the sample and the confocal lens in all confocal imaging.

Particle tracking routine

An iterative particle tracking procedure was used to extract particle positions from 3D datastacks. After a Gaussian smoothing, the color channels were incrementally thresholded and the centre of mass for each patch was determined using Wavemetrics 3D particle tracking implemented in *Igor Pro 8*. For each particle found, the coordinates were recorded, the local background around the patch was determined and a Gaussian shape was fitted in {x, y, z} to determine the width and amplitude of the patch intensity. Subsequently, a Gaussian spot of equally intensity and size was subtracted from the dataset and the threshold was lowered again until all patches were found. Patches and cores were paired by finding the nearest core for each patch with a distance cutoff of $r_{\text{cutoff}} = 800 \, \text{nm}$ (since for sample A, $r_{\text{core}} = 540$ and $r_{\text{patch}} = 125$) to ensure that all protrusions are captured and free-floating/non-paired protrusions are ignored. Finally, patch number distributions are calculated, as well as for each core particle the angles between each of its patches. The coordinate file was rendered in *POV-ray* version 3.7.

Simulations of patch number distributions

Monte Carlo simulations in the isothermalâĂŞisobaric ensemble (known as 'NPT') were performed to investigate to what extent the obtained patch number distributions are affected by polydispersity and maximum inter-particle separation (that still allows for size exclusion of the grafting molecules). Briefly, the initial configuration for each simulation was an FCC lattice with a volume fraction slightly above 0.5 and a log-normal distribution for a specific size polydispersity. The total system size was N = 2048. The configuration was then compressed until the volume fraction remained constant. Each simulation consisted of 10^5 cycles, and per cycle on average one attempt was carried out to change the volume by N-1 attempts to move a randomly chosen particle (with N = 2048). The particles are hard spheres (approximated by using a Yukawa potential with $\kappa\sigma \approx 1000$, where κ is the inverse Debye length and σ the average particle diameter) with a Yukawa potential and a

contact energy of $k_B T = 81$. Simulations were carried out for particle polydispersities 0%, 1%, 2%, 3%, 4% and 5%, with five independent simulations per polydispersity value. A particle (of radius R_1) was assumed to have a patch when the distance to its neighbor (of radius R_2) was smaller than $R_1 + R_2 + d$, in which d is a cut-off distance that depends on the grafting molecule size (i.e. the maximum distance between the surfaces of the particles which still excludes the grafting molecules due to their finite size). 'Rattlers', i.e. particles that could still move in a cage of other particles, were not moved downward in these simulations as they would experimentally on account of gravity. Simulations were performed for three values of d: 0.1%, 1% and 10% of the average particle diameter. The simulations returned the coordinates of the particles in the final configuration and, more importantly, histograms of the number of patches per particle (patch number distributions).

ASSOCIATED CONTENT

Acknowledgements

Author contributions statement

MK performed all experimental work (except PALM modification), initiated collaborations, and wrote the manuscript. BdN performed the TEM tomography reconstructions, and wrote the algorithm for particle tracking and extracting patch number distributions. MNvdL performed the simulations for theoretical patch number distributions. IdF performed functionalization with Cage 552, and IdF and AA performed PALM measurements. MJL synthesized micron-sized patchy silica particles with silica protrusions under supervision of MK. JPG helped to carry out particle tracking and FW helped obtain STED images. AvB designed research. IKV, JJB and AvB supervised research. The manuscript was approved by all authors.

Additional information

Competing financial interests The authors declare no competing financial interests.

Supplementary Information Additional figures; additional calculation; additional information on fluted silica rods, dye incorporation into silica protrusions, STED, PALM, titania polymorph characterization and solvophobic interactions; supporting videos and supporting references.

References

(1) Kraft, D. J.; Hilhorst, J.; Heinen, M. A. P.; Hoogenraad, M. J.; Luigjes, B.; Kegel, W. K. Patchy Polymer Colloids with Tunable Anisotropy Dimensions. *The Journal of Physical Chemistry B* **2011**, *115*, 7175–7181.

(2) Kraft, D. J.; Ni, R.; Smallenburg, F.; Hermes, M.; Yoon, K.; Weitz, D. A.; van Blaaderen, A.; Groenewold, J.; Dijkstra, M.; Kegel, W. K. Surface roughness directed self-assembly of patchy particles into colloidal micelles. **2012**, *109*, 10787–10792.

(3) Bianchi, E.; Kahl, G.; Likos, C. N.; Sciortino, F. Patchy particles. *Journal of Physics Condensed Matter* **2015**, *27*, no. 230301.

(4) Wang, Y.; Wang, Y.; Breed, D. R.; Manoharan, V. N.; Feng, L.; Hollingsworth, A. D.; Weck, M.; Pine, D. J. Colloids with valence and specific directional bonding. *Nature* **2012**, *491*, 51–55.

(5) van Blaaderen, A. Materials Science: Colloids get complex. *Nature* **2006**, *439*, 545–546.

(6) Sacanna, S.; Korpics, M.; Rodriguez, K.; Colón-Meléndez, L.; Kim, S.-H.; Pine, D. J.; Yi, G.-R. Shaping colloids for self-assembly. *Nature Communications* **2013**, *4*, no. 1688.

(7) Lunn, D. J.; Finnegan, J. R.; Manners, I. Self-assembly of "patchy" nanoparticles: a versatile approach to functional hierarchical materials. *Chemical Science* **2015**, *6*, 3663–3673.

(8) Kumar, A.; Park, B. J.; Tu, F.; Lee, D. Amphiphilic Janus particles at fluid interfaces. *Soft Matter* **2013**, *9*, 6604–6617.

(9) Yi, G.-R.; Pine, D. J.; Sacanna, S. Recent progress on patchy colloids and their self-assembly. *Journal of Physics: Condensed Matter* **2013**, *25*, no. 193101.

(10) Walther, A.; Müller, A. H. E. Janus Particles: Synthesis, Self-Assembly, Physical Properties, and Applications. *Chemical Reviews* **2013**, *113*, 5194–5261.

(11) Kaewsaneha, C.; Tangboriboonrat, P.; Polpanich, D.; Eissa, M.; Elaissari, A. Janus Colloidal Particles: Preparation, Properties, and Biomedical Applications. *ACS Applied Materials & Interfaces* **2013**, *5*, 1857–1869.

(12) Song, Y.; Chen, S. Janus Nanoparticles: Preparation, Characterization, and Applications. *Chemistry - An Asian Journal* **2014**, *9*, 418–430.

(13) Étienne Duguet,; Hubert, C.; Chomette, C.; Perro, A.; Ravaine, S. Patchy colloidal particles for programmed self-assembly. *Comptes Rendus Chimie* **2016**, *19*, 173–182.

(14) Elacqua, E.; Zheng, X.; Shillingford, C.; Liu, M.; Weck, M. Molecular Recognition in the Colloidal World. *Accounts of Chemical Research* **2017**, *50*, 2756–2766.

(15) Bianchi, E.; van Oostrum, P. D.; Likos, C. N.; Kahl, G. Inverse patchy colloids: Synthesis, modeling and self-organization. *Current Opinion in Colloid & Interface Science* **2017**, *30*, 8–15.

(16) Teixeira, P.; Tavares, J. Phase behaviour of pure and mixed patchy colloids – Theory and simulation. *Current Opinion in Colloid Interface Science* **2017**, *30*, 16–24.

(17) Bradley, L. C.; Chen, W.-H.; Stebe, K. J.; Lee, D. Janus and patchy colloids at fluid interfaces. *Current Opinion in Colloid & Interface Science* **2017**, *30*, 25–33.

(18) Porter, C. L.; Crocker, J. C. Directed assembly of particles using directional DNA interactions. *Current Opinion in Colloid & Interface Science* **2017**, *30*, 34–44.

(19) Ravaine, S.; Étienne Duguet, Synthesis and assembly of patchy particles: Recent progress and future prospects. *Current Opinion in Colloid & Interface Science* **2017**, *30*, 45–53.

(20) Petukhov, A. V.; Tuinier, R.; Vroege, G. J. Entropic patchiness: Effects of colloid shape and depletion. *Current Opinion in Colloid & Interface Science* **2017**, *30*, 54–61.

(21) Avendaño, C.; Escobedo, F. A. Packing, entropic patchiness, and self-assembly of non-convex colloidal particles: A simulation perspective. *Current Opinion in Colloid & Interface Science* **2017**, *30*, 62 – 69.

(22) Morphew, D.; Chakrabarti, D. Clusters of anisotropic colloidal particles: From colloidal molecules to supracolloidal structures. *Current Opinion in Colloid & Interface Science* **2017**, *30*, 70–80.

(23) Aubret, A.; Ramananarivo, S.; Palacci, J. Eppur si muove, and yet it moves: Patchy (phoretic) swimmers. *Current Opinion in Colloid & Interface Science* **2017**, *30*, 81–89.

(24) Jiang, S.; Van Dyk, A.; Maurice, A.; Bohling, J.; Fasano, D.; Brownell, S. Design colloidal particle morphology and self-assembly for coating applications. *Chemical Society Reviews* **2017**, *46*, 3792–3807.

(25) Sciortino, F.; Zaccarelli, E. Equilibrium gels of limited valence colloids. *Current Opinion in Colloid & Interface Science* **2017**, *30*, 90–96.

(26) Jo, I.-S.; Lee, S.; Zhu, J.; Shim, T. S.; Yi, G.-R. Soft patchy micelles. *Current Opinion in Colloid & Interface Science* **2017**, *30*, 97–105.

(27) Evers, C. H.; Luiken, J. A.; Bolhuis, P. G.; Kegel, W. K. Self-assembly of microcapsules via colloidal bond hybridization and anisotropy. *Nature* **2016**, *534*, 364–368.

(28) Bianchi, E.; Largo, J.; Tartaglia, P.; Zaccarelli, E.; Sciortino, F. Phase Diagram of Patchy Colloids: Towards Empty Liquids. *Phys. Rev. Lett.* **2006**, *97*, no. 168301.

(29) Chen, Q.; Bae, S. C.; Granick, S. Directed self-assembly of a colloidal kagome lattice. *Nature* **2011**, *469*, 381–384.

(30) Chen, Q.; Whitmer, J. K.; Jiang, S.; Bae, S. C.; Luijten, E.; Granick, S. Supracolloidal Reaction Kinetics of Janus Spheres. **2011**, *331*, 199–202.

(31) Morgan, J. W. R.; Chakrabarti, D.; Dorsaz, N.; Wales, D. J. Designing a Bernal Spiral from Patchy Colloids. *ACS Nano* **2013**, *7*, 1246–1256.

(32) Munaò, G.; Preisler, Z.; Vissers, T.; Smallenburg, F.; Sciortino, F. Cluster formation in one-patch colloids: low coverage results. *Soft Matter* **2013**, *9*, 2652–2661.

(33) Preisler, Z.; Vissers, T.; Smallenburg, F.; Munaò, G.; Sciortino, F. Phase Diagram of One-Patch Colloids Forming Tubes and Lamellae. *The Journal of Physical Chemistry B* **2013**, *117*, 9540–9547.

(34) Munaò, G.; O'Toole, P.; Hudson, T. S.; Costa, D.; Caccamo, C.; Giacometti, A.; Sciortino, F. Phase separation and self-assembly of colloidal dimers with tunable attractive strength: from symmetrical square-wells to Janus dumbbells. *Soft Matter* **2014**, *10*, 5269–5279.

(35) Preisler, Z.; Vissers, T.; Munaò, G.; Smallenburg, F.; Sciortino, F. Equilibrium phases of one-patch colloids with short-range attractions. *Soft Matter* **2014**, *10*, 5121–5128.

(36) Guo, R.; Mao, J.; Xie, X.-M.; Yan, L.-T. Predictive supracolloidal helices from patchy particles. **2014**, *4*, no. 7021.

(37) Vissers, T.; Smallenburg, F.; Munaò, G.; Preisler, Z.; Sciortino, F. Cooperative polymerization of one-patch colloids. *The Journal of Chemical Physics* **2014**, *140*, no. 144902.

(38) Munaò, G.; O'Toole, P.; Hudson, T. S.; Costa, D.; Caccamo, C.; Sciortino, F.; Giacometti, A. Cluster formation and phase separation in heteronuclear Janus dumbbells. *Journal of Physics: Condensed Matter* **2015**, *27*, no. 234101.

(39) Wolters, J. R.; Avvisati, G.; Hagemans, F.; Vissers, T.; Kraft, D. J.; Dijkstra, M.; Kegel, W. K. Self-assembly of "Mickey Mouse" shaped colloids into tube-like structures: experiments and simulations. *Soft Matter* **2015**, *11*, 1067–1077.

(40) Wolters, J. R.; Verweij, J. E.; Avvisati, G.; Dijkstra, M.; Kegel, W. K. Depletion-Induced Encapsulation by Dumbbell-Shaped Patchy Colloids Stabilize Microspheres against Aggregation. **2017**, *33*, 3270–3280.

(41) Munaò, G.; Costa, D.; Prestipino, S.; Caccamo, C. Aggregation of colloidal spheres mediated by Janus dimers: A Monte Carlo study. *Colloids and Surfaces A: Physicochemical and Engineering Aspects* **2017**, *532*, 397–404.

(42) Chaudhary, K.; Juareza, J. J.; Chen, Q.; Granick, S.; Lewis, J. A. Reconfigurable assemblies of Janus rods in AC electric fields. *Soft Matter* **2014**, *10*, 1320–1324.

(43) Shah, A. A.; Schultz, B.; Zhang, W.; Glotzer, S. C.; Solomon, M. J. Actuation of shape-memory colloidal fibres of Janus ellipsoids. *Nature Materials* **2015**, *14*, 117–124.

(44) Zhao, B.; Zhou, H.; Liu, C.; Long, Y.; Yang, G.; Tung, C.-H.; Song, K. Fabrication and directed assembly of magnetic Janus rods. *New J. Chem.* **2016**, *40*, 6541–6545.

(45) Yan, J.; Chaudhary, K.; Chul Bae, S.; Lewis, J. A.; Granick, S. Colloidal ribbons and rings from Janus magnetic rods. *Nature Communications* **2013**, *4*, no. 1516.

(46) Fan, W.; Liu, L.; Zhao, H. Co-assembly of patchy polymeric micelles and protein molecules. *Angewandte Chemie* **2017**, *56*, 8844–8848.

(47) Wang, L.; Xia, L.; Li, G.; Ravaine, S.; Zhao, X.-S. Patterning the Surface of Colloidal Microspheres and Fabrication of Nonspherical Particles. *Angewandte Chemie International Edition* **2008**, *47*, 4725–4728.

(48) Bae, C.; Kim, H.; Moreno, J. M. M.; Yi, G.-R.; Shin, H. Toward Coordinated Colloids: Site-Selective Growth of Titania on Patchy Silica Particles. *Scientific reports* **2015**, *5*, no. 9339.

(49) Wang, Y.; Wang, Y.; Zheng, X.; Étienne Ducrot,; Yodh, J. S.; Weck, M.; Pine, D. J. Crystallization of DNA-coated colloids. *Nature Communications* **2015**, *6*, no. 7253.

(50) Jiang, K.; Liu, Y.; Yan, Y.; Wang, S.; Liu, L.; Yang, W. Combined chain- and step-growth dispersion polymerization toward PSt particles with soft, clickable patches. *Polym. Chem.* **2017**, *8*, 1404–1416.

(51) Yan, W.; Pan, M.; Yuan, J.; Liu, G.; Cui, L.; Zhang, G.; Zhu, L. Raspberry-like patchy particles achieved by decorating carboxylated polystyrene cores with snowman-like poly(vinylidene fluoride)/poly(4-vinylpyridiene) Janus particles. *Polymer* **2017**, *122*, 139–147.

(52) Gong, Z.; Hueckel, T.; Yi, G.-R.; Sacanna, S. Patchy particles made by colloidal fusion. **2017**, *550*, 234–238.

(53) Mihut, A. M.; Stenqvist, B.; Lund, M.; Schurtenberger, P.; Crassous, J. J. Assembling oppositely charged lock and key responsive colloids: A mesoscale analog of adaptive chemistry. *Science Advances* **2017**, *3*, e1700321.

(54) Curk, T.; Dobnikar, J.; Frenkel, D. *Multivalency*; John Wiley and Sons, Ltd, 2017; Chapter 3, pp 75–101.

(55) Benyettou, F.; Zheng, X.; Elacqua, E.; Wang, Y.; Dalvand, P.; Asfari, Z.; Olsen, J.-C.; Han, D. S.; Saleh, N.; Elhabiri, M.; Weck, M.; Trabolsi, A. Redox-Responsive Viologen-Mediated Self-Assembly of CB[7]-Modified Patchy Particles. *Langmuir* **2016**, *32*, 7144–7150.

(56) Elacqua, E.; Zheng, X.; Weck, M. Light-Mediated Reversible Assembly of Polymeric Colloids. *ACS Macro Letters* **2017**, *6*, 1060–1065.

(57) Jang, S.; Kim, K.; Jeon, J.; Kang, D.; Sohn, B.-H. Supracolloidal chains of patchy micelles of diblock copolymers with in situ synthesized nanoparticles. *Soft Matter* **2017**, *13*, 6756–6760.

(58) Nguyen, T. A.; Newton, A.; Kraft, D. J.; Bolhuis, P. G.; Schall, P. Tuning Patchy Bonds Induced by Critical Casimir Forces. *Materials* **2017**, *10*, no. 1265.

(59) Zheng, X.; Liu, M.; He, M.; Pine, D. J.; Weck, M. Shape-Shifting Patchy Particles. *Angewandte Chemie* **2017**, *129*, 5599–5603.

(60) Bradley, L. C.; Stebe, K. J.; Lee, D. Clickable Janus Particles. *Journal of the American Chemical Society* **2016**, *138*, 11437–11440.

(61) Dias, C. S.; Tavares, J. M.; Araújo, N. A. M.; da Gama, M. M. T. Temperature driven dynamical arrest of a network fluid: the role of loops. *arXiv:1604.05279 [cond-mat.soft]*

(62) Zaccarelli, E. Colloidal gels: equilibrium and non-equilibrium routes. *Journal of Physics: Condensed Matter* **2007**, *19*, no. 323101.

(63) Tavares, J. M.; Dias, C. S.; Araújo, N. A. M.; Telo da Gama, M. M. Dynamics of Patchy Particles in and out of Equilibrium. *The Journal of Physical Chemistry B* **2018**, *122*, 3514–3518.

(64) Dias, C. a. S.; Araújo, N. A. M.; Telo da Gama, M. M. Non-equilibrium adsorption of 2AnB patchy colloids on substrates. *Soft Matter* **2013**, *9*, 5616–5623.

(65) Dias, C. S.; Araújo, N. A. M.; Telo da Gama, M. M. Nonequilibrium growth of patchy-colloid networks on substrates. *Phys. Rev. E* **2013**, *87*, 032308.

(66) Dias, C.; Araújo, N.; da Gama, M. T. Effect of the number of patches on the growth of networks of patchy colloids on substrates. *Molecular Physics* **2015**, *113*, 1069–1075.

(67) Tito, N.; Frenkel, D. Switch-like surface binding of competing multivalent particles. *The European Physical Journal Special Topics* **2016**, *225*, 1673–1682.

(68) Reinhardt, A.; Ho, C. P.; Frenkel, D. Effects of co-ordination number on the nucleation behaviour in many-component self-assembly. *Faraday Discuss.* **2016**, *186*, 215–228.

(69) Newton, A. C.; Groenewold, J.; Kegel, W. K.; Bolhuis, P. G. The role of multivalency in the association kinetics of patchy particle complexes. *The Journal of Chemical Physics* **2017**, *146*, no. 234901.

(70) Sciortino, F. Gel-forming patchy colloids and network glass formers: thermodynamic and dynamic analogies. *The European Physical Journal B* **2008**, *64*, 505–509.

(71) Russo, J.; Tartaglia, P.; Sciortino, F. Reversible gels of patchy particles: Role of the valence. *The Journal of Chemical Physics* **2009**, *131*, no. 014504.

(72) Sciortino, F.; Zaccarelli, E. Reversible gels of patchy particles. *Current Opinion in Solid State and Materials Science* **2011**, *15*, 246–253.

(73) Wang, G.; Swan, J. W. Surface heterogeneity affects percolation and gelation of colloids: dynamic simulations with random patchy spheres. *Soft Matter* **2019**, *15*, 5094–5108.

(74) Ruzicka, B.; Zaccarelli, E.; Zulian, L.; Angelini, R.; Sztucki, M.; Moussaïd, A.; Narayanan, T.; Sciortino, F. Observation of empty liquids and equilibrium gels in a colloidal clay. *Nature Materials* **2011**, *10*, 56–60.

(75) Bianchi, E.; Kahl, G.; Likos, C. N. Inverse patchy colloids: from microscopic description to mesoscopic coarse-graining. *Soft Matter* **2011**, *7*, 8313–8323.

(76) Stipsitz, M.; Kahl, G.; Bianchi, E. Generalized inverse patchy colloid model. *The Journal of Chemical Physics* **2015**, *143*, no. 114905.

(77) Ferrari, S.; Bianchi, E.; Kalyuzhnyi, Y. V.; Kahl, G. Inverse patchy colloids with small patches: fluid structure and dynamical slowing down. *Journal of Physics: Condensed Matter* **2015**, *27*, no. 234104.

(78) van Oostrum, P. D. J.; Hejazifar, M.; Niedermayer, C.; Reimhult, E. Simple method for the synthesis of inverse patchy colloids. *Journal of Physics: Condensed Matter* **2015**, *27*, no. 234105.

(79) Sabapathy, M.; Ann Mathews K, R.; Mani, E. Self-assembly of inverse patchy colloids with tunable patch coverage. *Phys. Chem. Chem. Phys.* **2017**, *19*, 13122–13132.

(80) Bernal, J. D.; Mason, J. Packing of Spheres: Co-ordination of Randomly Packed Spheres. *Nature* **1960**, *188*, 910–911.

(81) van Blaaderen, A.; Wiltzius, P. Template-directed colloidal crystallization. *Science* **1995**, *270*, 1177–1179.

(82) Midgley, P. A.; Dunin-Borkowski, R. E. Electron tomography and holography in materials science. *Nature Materials* **2009**, *8*, 271–280.

(83) Pronk, S.; Frenkel, D. Point defects in hard-sphere crystals. *The Journal of Physical Chemistry B* **2001**, *105*, 6722–6727.

(84) Kuijk, A.; van Blaaderen, A.; Imhof, A. Synthesis of Monodisperse, Rodlike Silica Colloids with Tunable Aspect Ratio. *Journal of the American Chemical Society* **2011**, *133*, 2346–2349.

(85) Peng, B.; Soligno, G.; Kamp, M.; de Nijs, B.; de Graaf, J.; Dijkstra, M.; van Roij, R.; van Blaaderen, A.; Imhof, A. Site-specific growth of polymers on silica rods. *Soft Matter* **2014**, *10*, 9644–9650.

(86) Míguez, H.; Meseguer, F.; López, C.; Blanco, A.; Moya, J. S.; Requena, J.; Mifsud, A.;

Fornés, V. Control of the Photonic Crystal Properties of fcc-Packed Submicrometer SiO₂ Spheres by Sintering. *Advanced Materials* **1998**, *10*, 480–483.

(87) Chabanov, A. A.; Jun, Y.; Norris, D. J. Avoiding cracks in self-assembled photonic band-gap crystals. *Applied Physics Letters* **2004**, *84*, 3573–3575.

(88) Shrivastava, V. P.; Kumar, J.; Sivakumar, S. On the controlled isotropic shrinkage induced fine-tuning of photo-luminescence in terbium ions embedded silica inverse opal films. *AIP Advances* **2017**, *7*, no. 125027.

(89) Van Blaaderen, A.; Vrij, A. Synthesis and characterization of colloidal dispersions of fluorescent, monodisperse silica spheres. *Langmuir* **1992**, *8*, 2921–2931.

(90) Mačković, M.; Niekiel, F.; Wondraczek, L.; Spiecker, E. Direct observation of electron-beam-induced densification and hardening of silica nanoballs by in situ transmission electron microscopy and finite element method simulations. *Acta Materialia* **2014**, *79*, 363–373.

(91) Mačković, M.; Niekiel, F.; Wondraczek, L.; Bitzek, E.; Spiecker, E. In situ mechanical quenching of nanoscale silica spheres in the transmission electron microscope. *Scripta Materialia* **2016**, *121*, 70–74.

(92) Demirörs, A. F.; van Blaaderen, A.; Imhof, A. Synthesis of Eccentric Titania-Silica Core-Shell and Composite Particles. *Chem. Mater.* **2009**, *21*, 979–984.

(93) Lawrie, G.; Grøndahl, L.; Battersby, B.; Keen, I.; Lorentzen, M.; Surawski, P.; Trau, M. Tailoring Surface Properties To Build Colloidal Diagnostic Devices: Controlling Interparticle Associations. *Langmuir* **2006**, *22*, 497–505.

(94) de Feijter, I.; Albertazzi, L.; Palmans, A. R.; Voets, I. K. Stimuli-Responsive Colloidal Assembly Driven by Surface-Grafted Supramolecular Moieties. *Langmuir* **2015**, *31*, 57–64.

(95) Vilanova, N.; de Feijter, I.; Teunissen, A. J. P.; Voets, I. K. Light induced assembly and self-sorting of silica microparticles. *Scientific Reports* **2018**, *8*, no. 1271.

(96) Demirörs, A. F.; van Blaaderen, A.; Imhof, A. A General Method to Coat Colloidal Particles with Titania. *Langmuir* **2010**, *26*, 9297–9303.

(97) Panwar, K.; Jassal, M.; Agrawal, A. K.

(98) Palacci, J.; Sacanna, S.; Kim, S.-H.; Yi, G.-R.; Pine, D. J.; Chaikin, P. M. Light-activated self-propelled colloids. *Philosophical Transactions of the Royal Society A: Mathematical, Physical and Engineering Sciences* **2014**, *372*, no. 20130372.

(99) Weast, R. *Handbook of Chemistry & Physics*, 65th ed.; CRC Press.

(100) Brinker, C. Hydrolysis and condensation of silicates: Effects on structure. *Journal of Non-Crystalline Solids* **1988**, *100*, 31–50.

(101) Harris, M. T.; Brunson, R. R.; Byers, C. H. The base-catalyzed hydrolysis and condensation reactions of dilute and concentrated TES solutions. *Journal of Non-Crystalline Solids* **1990**, *121*, 397–403.

(102) Bogush, G.; Zukoski IV, C. Studies of the kinetics of the precipitation of uniform silica particles through the hydrolysis and condensation of silicon alkoxides. *Journal of Colloid and Interface Science* **1991**, *142*, 1–18.

(103) Liu, B.; Besseling, T. H.; Hermes, M.; DemirÃűrs, A. F.; Imhof, A.; van Blaaderen, A. Switching plastic crystals of colloidal rods with electric fields. *Nature Communications* **2014**, *5*, 3092.

(104) Vlug, W. S. *Balls, beams and blocks: In situ observation of colloidal particles in confinement and under electron irridiation.*; Utrecht University, 2017.

(105) Kamp, M.; Elbers, N. A.; Troppenz, T.; Imhof, A.; Dijkstra, M.; van Roij, R.; van Blaaderen, A. Electric-Field-Induced Lock-and-Key Interactions between Colloidal Spheres and Bowls. *Chemistry of Materials* **2016**, *28*, 1040–1048.

(106) Elbers, N. A.; Jose, J.; Imhof, A.; van Blaaderen, A. Bulk Scale Synthesis of Monodisperse PDMS Droplets above three micrometer and Their Encapsulation by Elastic Shells. *Chemistry of Materials* **2015**, *27*, 1709–1719.

(107) Kraft, D. J.; Vlug, W. S.; van Kats, C. M.; van Blaaderen, A.; Imhof, A.; Kegel, W. K. Self-Assembly of Colloids with Liquid Protrusions. *Journal of the American Chemical Society* **2009**, *131*, 1182–1186.

(108) Cho, Y.-S.; Yi, G.-R.; Kim, S.-H.; Elsesser, M. T.; Breed, D. R.; Yang, S.-M. Homogeneous and heterogeneous binary colloidal clusters formed by evaporation-induced self-assembly inside droplets. *Journal of Colloid & Interface Science* **2008**, *318*, 124–133.

(109) Qiu, P.; Mao, C. Viscosity Gradient as a Novel Mechanism for the Centrifugation-Based Separation of Nanoparticles. *Advanced Materials* **2011**, *23*, 4880–4885.

(110) van der Linden, M. N.; El Masri, D.; Dijkstra, M.; van Blaaderen, A. Expansion of charged colloids after centrifugation: formation and crystallisation of long-range repulsive glasses. *Soft Matter* **2013**, *9*, 11618–11633.

(111) Verhaegh, N. A. M.; Blaaderen, A. v. Dispersions of rhodamine-labeled silica spheres: synthesis, Characterization, and Fluorescence Confocal Scanning Laser Microscopy. *Langmuir* **1994**, *10*, 1427–1438.

(112) Giesche, H. Synthesis of monodispersed silica powders II. Controlled growth reaction and continuous production process. *Journal of the European Ceramic Society* **1994**, *14*, 205–214.

(113) Bogush, G.; Tracy, M.; Zukoski IV, C. Preparation of monodisperse silica particles: Control of size and mass fraction. *Journal of Non-Crystalline Solids* **1988**, *104*, 95–106.

(114) Petukhov, A. V.; Thijssen, J. H. J.; Imhof, A.; van Blaaderen, A.; I. Dolbnya, P.; Snigirev, A.; Snigireva, I.; Drakopoulos, M. 3D structure and dis-(order) in photonic crystals by microradian synchrotron X-ray diffraction. *ESRF Newsletter* **2003**, *38*, 19–20.

(115) Thijssen, J. H. J.; Petukhov, A. V.; 't Hart, D. C.; Imhof, A.; van der Werf, C. H. M.; Schropp, R. E. I.; van Blaaderen, A. Characterization of Photonic Colloidal Single Crystals by Microradian X-ray Diffraction. *Advanced Materials* **2006**, *18*, 1662–1666.

(116) Petukhov, A. V.; Thijssen, J. H. J.; 't Hart, D. C.; Imhof, A.; van Blaaderen, A.; Dolbnya, I. P.; Snigirev, A.; Moussaïd, A.; Snigireva, I. Microradian X-ray diffraction in colloidal photonic crystals. *Journal of Applied Crystallography* **2006**, *39*, 137–144.

(117) Mooney, J. F.; Hunt, A. J.; McIntosh, J. R.; Liberko, C. A.; Walba, D.; Rogers, C. Patterning of functional antibodies and other proteins by photolithography of silane monolayers. *Proceedings of the National Academy of Sciences* **1996**, *93*, 12287–12291.

(118) Vogel, B. M.; DeLongchamp, D. M.; Mahoney, C. M.; Lucas, L. A.; Fischer, D. A.; Lin, E. K. Interfacial modification of silica surfaces through γ-isocyanatopropyl triethoxy silane-amine coupling reactions. *Applied Surface Science* **2008**, *254*, 1789–1796.

(119) Bae, C.; Moon, J.; Shin, H.; Kim, J.; Sung, M. M. Fabrication of Monodisperse Asymmetric Colloidal Clusters by Using Contact Area Lithography (CAL). *J. Am. Chem. Soc.* **2007**, *129*, 14232–14239.

(120) Bozzola, J. J.; Russell, L. D. Electron Microscopy: Principles and Techniques for Biologists. **1999**,

(121) Friedrich, H.; Gommes, C. J.; Overgaag, K.; Meeldijk, J. D.; Evers, W. H.; de Nijs, B.; Boneschanscher, M. P.; de Jongh, P. E.; Verkleij, A. J.; de Jong, K. P.; van Blaaderen, A.; Vanmaekelbergh, D. Quantitative Structural Analysis of Binary Nanocrystal Superlattices by Electron Tomography. *Nano Letters* **2009**, *9*, 2719–2724.

(122) de Nijs, B.; Dussi, S.; Smallenburg, F.; Meeldijk, J. D.; Groenendijk, D. J.; Filion, L.; Imhof, A.; van Blaaderen, A.; Dijkstra, M. Entropy-driven formation of large icosahe-dral colloidal clusters by spherical confinement. *Nature Materials* **2015**, *14*, 56–60.

(123) Durrani, T.; Bisset, D. The Radon transform and its properties. *Geophysics* **1984**, *49*, 1180–1187.

(124) Radermacher, M. Three-dimensional reconstruction from random projections: orientational alignment via Radon transforms. *Ultramicroscopy* **1994**, *53*, 121–136.

(125) Natterer, F. *The Mathematics of Computerized Tomography*; Vieweg+Teubner Verlag, 1986.

(126) Besseling, T.; Jose, J.; van Blaaderen, A. Methods to calibrate and scale axial distances in confocal microscopy as a function of refractive index. *Journal of Microscopy* **2015**, *257*, 142–150.